

An emergent community ecosystem model applied to the California Current System

Nicole L. Goebel^a, Christopher A. Edwards^{b,*}, Jonathan P. Zehr^b,
Mick Follows^c

^a*Institute of Marine Sciences, University of California, Santa Cruz, CA, 95064, U.S.A*

^b*Ocean Sciences Department, University of California, Santa Cruz, CA, 95064, U.S.A*

^c*Department of Earth, Atmospheric and Planetary Sciences, Massachusetts Institute of Technology, Cambridge, MA, 02139, U.S.A*

Abstract

An ecosystem model that supports considerable phytoplankton diversity is coupled to a circulation model of the California Current System. The Regional Ocean Modeling System is configured for a realistic simulation at 0.1 degree resolution for years 2000-2004. The concentration-based ecosystem model includes multiple nutrients, dissolved and particulate organic pools, two grazers, and 78 phytoplankton. Primary producers divide into 4 functional groups representing diatoms, large phytoplankton that do not require silicate, *Prochlorococcus*-like organisms, and small phytoplankton that can use nitrate. Random selection of phytoplankton growth parameters creates an autotrophic community able to fill multiple environmental niches created by the physical circulation. In the 5-year average, over 98% of the total biomass at the surface is contained within 8 primary producers, with 30

*Corresponding author

Email addresses: ngoebel@ucsc.edu (Nicole L. Goebel), cedwards@ucsc.edu (Christopher A. Edwards), zehrj@pmc.ucsc.edu (Jonathan P. Zehr), mick@ocean.mit.edu (Mick Follows)

additional phytoplankton sustained at lower levels. Modeled surface phytoplankton biomass is evaluated on multi-annual and seasonal bases using satellite chlorophyll estimates for the same period. The self-organized communities produced by the model represent various features of the California Current Ecosystem, including the biogeographic break at Pt. Conception. The annual average fields generally reveal high diatom concentrations nearshore, with small phytoplankton more broadly distributed. *Prochlorococcus*-like organisms are absent or at very low concentrations at the coast, increasing across the California Current. Small non-*Prochlorococcus*-like phytoplankton are found at highest concentrations nearshore and far offshore. The model exhibits both surface and subsurface features, including a seasonal subsurface chlorophyll maximum along CalCOFI Line 67 between May and October. Time-series of area-averaged model fields show succession of different phytoplankton groups over the annual cycle.

1. Introduction

One challenge for modeling ocean ecosystems is representing the remarkable diversity of marine planktonic organisms. In nature, such diversity is revealed by observations of multiple species at varying biomass concentrations and having differing community structure within spatially or temporally distinct biogeographical domains. Ever improving observational approaches have over time increased documentation of oceanic species. Identifying subspecies differentiation is now routine through the use of molecular techniques. How such diversity in the ocean is sustained given the small number of limiting nutrients remains a long-standing scientific question (Hutchinson, 1961;

11 Roy and Chattopadhyay, 2007), and our understanding of its impact on over-
12 all ecosystem dynamics and net biological production remains incomplete. If
13 ecosystem models are able to represent the complex heterogeneous plank-
14 tonic diversity in the ocean, they represent one method to investigate and
15 better understand the underlying causes and impacts.

16 Historically, concentration-based ocean ecosystem models have addressed
17 biodiversity minimally, typically budgeting phytoplankton, for example, through
18 the use of one or a small number of functional groups that implicitly represent
19 many different phytoplankton species. Among the simplest of these models
20 is the *NPZ* model (e.g., Franks, 2002), which includes one nutrient (*N*), one
21 phytoplankton type (*P*), and one zooplankton (*Z*). More complex variants
22 (Fasham et al., 1990; Gruber et al., 2006) include two nutrient compartments
23 as well as one or two detrital pools. Other models (e.g., Chai et al., 2002;
24 Moore et al., 2002a; Litchman et al., 2006) expand phytoplankton into two
25 functional groups and zooplankton into one, two, or three boxes. All models
26 described have been valuable tools to study ocean ecosystems in different
27 contexts, and choosing the appropriate level of model complexity has been
28 considered typically on a problem dependent basis. Taken as a series, these
29 examples highlight the fact that over decades traditional ecosystem models
30 have evolved in systematic but incremental progression, resolving only a very
31 small amount of total planktonic diversity.

32 An alternate approach toward ecosystem model construction has been
33 developed recently (Follows et al., 2007). At its core, this type of emergent
34 community ecosystem model is not fundamentally different from the more
35 traditional type. It solves a series of coupled nonlinear differential equations

36 quantifying changes in time for biological and chemical concentrations with
37 formulations similar to other models. However, this approach is unique both
38 in the large number ($O(100)$) of viable phytoplankton fields included and in
39 the method by which some rate-controlling parameters are set.

40 In traditional *NPZ*-type models, parameters that control growth, graz-
41 ing, and remineralization processes are precisely chosen by the modeler. At
42 times, this selection is made with careful attention to observations or field
43 studies appropriate for a particular region (Banas et al., 2009), but some
44 parameters (e.g., zooplankton mortality) are not easily measured, and the
45 value used is less constrained. Other parameters, such as the sensitivity of
46 growth rate to ambient temperature, show substantial scatter (Eppley, 1972;
47 Brush et al., 2002); choosing a single value may not represent the breadth of
48 values found in nature within a functional group. Furthermore, underlying
49 model evolution can be sensitive to parameter choice (Edwards et al., 2000b).
50 In the Follows et al. (2007) approach, some rate-controlling parameters are
51 fixed as in more traditional cases, but others are randomly chosen within rea-
52 sonable limits given observational scatter. Thus the model ocean is seeded
53 with a large number of independent phytoplankton species or subspecies,
54 each with its own growth parameters and able to compete individually for
55 available resources. Applied to the global ocean, this model resolved latitu-
56 dinal structure for 3 ecotypes of *Prochlorococcus* spp. similar to that found
57 along the Meridional Atlantic Transect (Follows et al., 2007; Johnson et al.,
58 2006). The structure derived from differing temperature and light environ-
59 ments in different oceanic regions combined with the availability within the
60 model of organisms able to utilize resources efficiently in the differing en-

61 vironmental niches. Microbial populations and underlying processes have
62 typically been neglected by more traditional modeling exercises, and the Fol-
63 lows et al. (2007) model is among the first to represent these explicitly in a
64 fully prognostic fashion.

65 Like their global ocean counterparts, coastal regions also exhibit a range
66 of chemical and physical environments owing to the presence of an oceanic
67 boundary and the changes with cross-shore distance in the large-scale circu-
68 lation, mesoscale variability, sub-mesoscale motion, and vertical mixing. The
69 California Current System, off the west coast of the United States, includes
70 such variations in oceanic environments, and evidence suggests considerable
71 planktonic diversity regionally, particularly between seasonally varying, often
72 nutrient replete, upwelled waters nearshore and oligotrophic offshore waters
73 (e.g., Venrick, 2009).

74 In this paper, we investigate the potential for the Follows et al. (2007)
75 model to represent the biogeography and biodiversity of the California Cur-
76 rent System. The model is seeded with 78 viable phytoplankton types that
77 can be collated into four functional groups. Physiological traits (e.g., nutri-
78 ent utilization and affinity, and response to temperature and light) for each
79 phytoplankton are randomly assigned from a range of values drawn from the
80 literature. With this approach, multiple, viable phytoplankton types com-
81 pete for resources, enabling a self-organizing phytoplankton community to
82 emerge. In Section 2 we describe the model, its components, and both fixed
83 and randomized biological parameterizations. Section 3 presents results, in-
84 cluding a quantitative model evaluation and descriptions of the surface and
85 subsurface fields, both time-averaged and over an annual cycle. We conclude

86 in Section 4 with a discussion of the results in context with CCS observations.

87 **2. Model Formulation**

88 *2.1. Emergent Community Ecosystem Model*

89 The ecosystem model is derived from the original, global-scale version of
90 Follows et al. (2007). The model is schematically shown in Figure 1. Multiple
91 phytoplankton populations access five inorganic nutrients (NO_3 , NO_2 , NH_4 ,
92 PO_4 , Si(OH)_4) and are grazed by two different sized zooplankton. Transfers
93 from phytoplankton and zooplankton populations to dissolved and partic-
94 ulate pools represent respiration, mortality, excretion, and sloppy feeding.
95 Dissolved and particulate constituents are remineralized into inorganic form.
96 The equations that govern the evolution of the ecosystem components are
97 provided in the Appendix and parameters are presented in Tables A.1, A.2,
98 and A.3.

99 Our model is seeded with 78 individual phytoplankton types that are ran-
100 domly subdivided. Phytoplankton are first divided approximately equally
101 into small and large size classes. Large phytoplankton are similarly subdivi-
102 ded into one group, representing diatoms, that require silicate for growth,
103 and a second category, referred to as LND (large non-diatoms), that does
104 not use silicate. Small phytoplankton are split into three different groups
105 according to their nitrogen utilization. Roughly one third of small phyto-
106 plankton use both NH_4 and NO_2 , one third use NH_4 only, and the remainder
107 can take up NH_4 , NO_2 , and NO_3 . We refer to these small phytoplankton as
108 SP1, SP2, and SP3, respectively. For analysis described in this paper, SP1
109 and SP2 are grouped into a category referred to as PLP (*Prochlorococcus*-like

110 phytoplankton), which are thought to primarily use NH_4 and NO_2 (Moore
111 et al., 2002b). SP3 is assumed to include all other small prokaryotes and
112 eukaryotes, and we refer to this group as SNP (Small Non-*Prochlorococcus*-
113 like). For clarity below, we refer to organisms within a particular functional
114 group as subtypes as our categorization can not distinguish between differ-
115 ent ecotypes of a single species and entirely different taxa within a particular
116 functional group.

117 Large phytoplankton are assigned faster maximum growth rates than
118 small phytoplankton. Diatoms are an important functional group in coastal
119 upwelling systems, and studies frequently report diatom growth rates that
120 exceed the community average (Chan, 1978, 1980; Brand, 1981; Brand and
121 Guillard, 1981; Furnas, 1990, 1991). For diatoms, we use a maximum diel-
122 averaged growth rate of approximately 3.6 divisions per day, near the upper
123 end of the net growth rates reported by Furnas (1990). Studies of maximum
124 net growth rate for large non-diatoms, such as dinoflagellates, have been
125 found in the same range but generally lower than that of diatoms (Chan,
126 1978; Weiler and Eppley, 1979; Chan, 1980), and our value corresponds to
127 a maximum 2.9 doublings per day. Small phytoplankton are allowed to di-
128 vide at a maximum of 2 times per day; this value is somewhat higher than
129 that implied by the culture experiments for *Synechococcus* and *Prochlorococ-*
130 *cus* (Moore et al., 2002b), but similar to the maximum net growth rates for
131 picoeukaryotes in dilution-based studies by Worden et al. (2004).

132 We note that the maximum growth rates listed in Table A.1 are twice
133 those normally reported and implied by the preceding discussion; however,
134 in our model these values result in approximately equivalent daily averaged

135 growth. Phytoplankton growth depends on incident photosynthetically ac-
 136 tive radiation which undergoes diel variations in our model configuration.
 137 Literature-based rates are obtained usually from laboratory measurements
 138 over a 24-hour period. Figure 2 compares the time-evolution of phytoplank-
 139 ton biomass for two simplified models including only uptake and respiration
 140 (no grazing). In both experiments, nutrients are plentiful, and the respira-
 141 tion rate is 0.1 d^{-1} . The dashed curve results from a growth rate of 1.4 d^{-1}
 142 and a light field that is constant with time. The solid curve corresponds to
 143 a growth rate of 2.8 d^{-1} but with a light field that varies as a step function
 144 between day and night cycles (dotted line). While respiration occurs at all
 145 times (Marra and Barber, 2004), it is most evident in the solid curve during
 146 nighttime. It is clear that the net increase in phytoplankton biomass in our
 147 two experiments is roughly equivalent over multiple days of growth.

148 Generally, realized phytoplankton growth is less than the maximum pos-
 149 sible rate resulting from modeled limitations associated with nutrient concen-
 150 trations, ambient temperature, and local light intensity. The four parameters
 151 that control these environmental responses are the half-saturation constants
 152 for uptake of each nutrient (generically referred to here as k_x), a tempera-
 153 ture optimum (T_o) and two light optimum parameters (k_{inh} and k_{par}). These
 154 parameters are determined randomly for each phytoplankton analog.

155 Nutrient limitation by inorganic phosphate and silicic acid is expressed
 156 using Michaelis-Menten kinetics. Inorganic nitrogen limitation is functionally
 157 similar, but quantitatively determined for each form of nitrogen assimilated.
 158 Oxidized forms of nitrogen are theorized to be more energetically expensive
 159 to assimilate, and their uptake is inhibited by the presence of ammonium in

160 the model (Nianzhi, 1993; L’Helguen et al., 2008). Phytoplankton growth is
 161 reduced by the most limiting nutrient resource. Half-saturation constants for
 162 phosphorous are related to those for nitrate and nitrite by a fixed Redfield
 163 Ratio. Half-saturation constants for ammonium are one half those for nitrite
 164 or nitrate; a higher affinity for NH_4 than NO_3 (Dugdale and Goering, 1967;
 165 Eppley et al., 1969; Conway, 1977) has been reported in small phytoplank-
 166 ton such as green algae (Litchman et al., 2007). The half-saturation constant
 167 for silicate is fixed for diatoms, while that for phosphorous and other stoi-
 168 chiometrically related nutrients are drawn from uniform distributions hav-
 169 ing size-dependent ranges (Table A.1). Large phytoplankton typically have
 170 higher k_x than small phytoplankton (Eppley et al., 1969).

171 Realized phytoplankton growth is also modified by local temperature,
 172 with warmer conditions generally enabling faster growth rates. However,
 173 each phytoplankton analog is individually and randomly prescribed a tem-
 174 perature optimum, T_o . This value, along with a specified temperature decay
 175 scale, T_d , defines a phytoplankton-specific temperature window for growth
 176 within a broader temperature limitation curve. The optimum is drawn from
 177 a uniform distribution between specified minimum and maximum tempera-
 178 tures characteristic of the CCS (Table A.1). This approach generates warm
 179 and cold adapted phytoplankton types in both size classes.

180 Finally, light limitation of phytoplankton growth is determined by the
 181 local photosynthetically active radiation and two parameters: k_{par} governs
 182 the limitation function under low-light conditions, and k_{inh} controls growth
 183 when solar radiation is high. Chloroplast placement due to packaging effects
 184 observed in large phytoplankton (Finkel, 2001) justifies a high light optimum

185 (i.e., low k_{inh} and a narrow range of k_{par}). Small phytoplankton have been
 186 observed to grow optimally at a wider range of light levels due to the pres-
 187 ence of both high and low light-adapted strains (Veldhuis et al., 2005), and
 188 therefore were assigned a wider range of light optima. The distributions from
 189 which light parameters for large and small phytoplankton are drawn, how-
 190 ever, overlap (Table A.1), and therefore such generalizations can occasionally
 191 be reversed. The light limitation model includes self-shading but does not
 192 resolve spectral bands.

193 The remaining ecosystem model parameters that describe phytoplank-
 194 ton losses (mortality, export and sinking) and heterotrophic processes (zoo-
 195 plankton grazing, sinking of particulates, particulate and dissolved organic
 196 matter remineralization, and nitrification) are fixed rather than randomly
 197 prescribed. See Appendix for the formulations.

198 Export and sinking of phytoplankton are size-specific. The rates for these
 199 processes are greater for large phytoplankton than for small phytoplankton.
 200 Mortality rates are set equal for all phytoplankton.

201 Two grazers are included in the model, and their parameters are not
 202 drawn from a random distribution of values. Change in biomass for each
 203 zooplankton is modeled using a sigmoidal grazing scheme (Gentleman et al.,
 204 2003), dependent on a maximum grazing rate (G^{max}), assimilation efficiency
 205 (α), and prey palatability (π) (Table A.2). The maximum grazing rate is
 206 size-specific. Mesozooplankton G^{max} is smaller than the microzooplankton
 207 rate (e.g., Leising et al., 2005a). Grazing varies also with the palatability and
 208 assimilation efficiency of the prey. Microzooplankton and large non-diatoms
 209 are parameterized as highly palatable to mesozooplankton, and small phyto-

210 plankton are highly palatable to microzooplankton. Diatoms are less palat-
211 able to all zooplankton within the model, as supported by evidence of the
212 size, shape, ornamentation, exudates, and accessibility of their siliceous frus-
213 trule. Small phytoplankton populations are modeled as least palatable to
214 mesozooplankton, and large phytoplankton are of medium palatability for
215 microzooplankton. Assimilation efficiencies are highest for mesozooplank-
216 ton consuming small phytoplankton, medium for phytoplankton grazing by
217 like-sized zooplankton, and lowest for microzooplankton ingesting large phy-
218 toplankton. Grazing of microzooplankton by mesozooplankton is included
219 providing potential relief of grazing pressure on the prey of the microzoo-
220 plankton, as observed in nature (e.g., Leising et al., 2005b). Modeled zoo-
221 plankton stoichiometry is allowed to vary, as opposed to the Redfield-based
222 ratio of phytoplankton. Zooplankton mortality obeys a linear relationship
223 with biomass.

224 In addition to the two explicitly modeled grazers, the heterotrophic com-
225 ponent also includes an implicit representation of microbes that remineralize
226 dissolved and particulate organic detrital pools that accumulate from the
227 mortality and excretion of phytoplankton and zooplankton (Figure 1). Rem-
228 ineralization of organic matter varies linearly with its concentration. Or-
229 ganic phosphorous is remineralized into phosphate, while organic nitrogen
230 is remineralized into ammonium, which is then nitrified to nitrite and then
231 to nitrate. Nitrification is modeled as a linear function with fixed coeffi-
232 cients (Table A.3). Rate parameters for remineralization processes are based
233 on sensitivity tests of literature-based values. There is no dissolved silicate
234 pool, and particulate silica is converted to the inorganic pool.

235 Care is taken to reduce all biological transfers between ecosystem compo-
236 nents when a calculated transfer in a discrete time-step exceeds the amount
237 available plus a very small baseline level. In this way, biological processes
238 maintain positive-definite quantities, the ecosystem model is conservative,
239 and very small seed populations remain for future growth.

240 For comparison to observed biomass estimates, modeled biomass in μmole
241 phosphorous liter^{-1} is converted to carbon using a Redfield ratio and then to
242 $\text{mg chlorophyll m}^{-3}$ as follows. The carbon to chlorophyll ratio, C:Chl, is rep-
243 resented as a constant value for each functional group. Phytoplankton C:Chl
244 ratios (as g C g chl^{-1}) reported in the literature range from values of 10 to
245 more than 700. Interspecific variation in C:Chl ratios of phytoplankton have
246 been shown to vary across conditions of light, nutrients, and temperature
247 (Geider, 1987). C:Chl ratios within a functional group however, are relatively
248 consistent, ranging from high values for oligotrophic, low-chlorophyll regions
249 (Buck et al., 1996) and low values for larger phytoplankton in eutrophic en-
250 vironments (Geider, 1987). C:Chl ratios exceeding 300 have been observed
251 in oligotrophic waters where small phytoplankton predominate (Buck et al.,
252 1996; Chavez et al., 1996; Chang et al., 2003; Veldhuis and Kraay, 2004) and
253 were observed to reach values of 300 in waters that contained only small phy-
254 toplankton cells ($<5 \mu\text{m}$) (Putland and Iverson, 2007). We used a C:Chl ratio
255 of 300 to represent the small phytoplankton in our model. Diatom-specific
256 C:Chl found throughout the literature falls within the lower range of ratios,
257 from 15 to 46 (Chan, 1980; Geider, 1987; Gallegos and Vant, 1996), while
258 the C:Chl ratio in eutrophic environments ranged from 16 to 83, most of
259 which fell between 27 and 67 mg C mg chl^{-1} (Riemann et al., 1989; Sathyen-

260 dranath et al., 2009). We represent coastal diatoms with a C:Chl ratio of 50,
 261 a middle value within this range. Reports of C:Chl ratios for dinoflagellates
 262 fall between that of small phytoplankton and large diatoms. Geider (1987)
 263 measured a range of 20 to 140 and Chan (1980) measured a range of 90 to
 264 120, while Sathyendranath et al. (2009) measured a range of 27 to 80 in
 265 Tokyo Bay. Based on these ranges for dinoflagellates which exceed those for
 266 diatoms, we apply a C:Chl of 100 for large non-diatoms. Gruber et al. (2006)
 267 applied a variable C:Chl ratio in their ecosystem model of the CCS. Resultant
 268 C:Chl in their model demonstrated onshore values of 40 and offshore
 269 values of 100, which fall within the ranges chosen here. Gruber et al. (2006)
 270 demonstrated the small benefit of utilizing a modeled C:Chl ratio when compared
 271 to using the average modeled value for the photic zone in instances
 272 where one is concerned only with surface chlorophyll concentrations. They
 273 found that a canonical, constant value of 40 would have largely impacted
 274 both the depth distributions and the relative onshore-offshore chlorophyll
 275 concentrations. In the present study, we also find a variable ratio important
 276 in estimating chlorophyll concentrations associated with small phytoplankton
 277 offshore, though our variability is expressed on a functional group basis.

278 *2.2. Physical model and coupled model conditions*

279 The ecosystem model is embedded within a physical circulation model of
 280 the California Current System. We use the Regional Ocean Modeling System (ROMS)
 281 configured for the CCS. Our implementation extends from the
 282 middle of the Baja California Peninsula to Vancouver Island and over 1000
 283 km offshore at 1/10 degree resolution and 42 vertical, topography-following
 284 levels. The model is forced at the surface by atmospheric fields from a high-

285 resolution atmospheric model (COAMPSTM, provided by the Naval Research
 286 Laboratory). Lateral boundary conditions are obtained from output from the
 287 global ocean state estimate ECCO (Estimating the Circulation and Climate
 288 of the Ocean). Details of the forward physical circulation model, its quan-
 289 titative comparison to observations, and its sensitivities to local and remote
 290 forcing are provided in Veneziani et al. (2009a,b). Additional information
 291 relating to how the forward model circulation changes as a result of regional
 292 data assimilation can be found in Broquet et al. (2009). The primary dif-
 293 ference between the physical implementation in the present study and those
 294 previously documented is the application of a positive definite tracer ad-
 295 vection scheme as opposed to a third-order upstream tracer advection. We
 296 use the Multidimensional Positive Definite Advection Transport Algorithm
 297 (MPDATA; Smolarkiewicz and Margolin, 1998). A positive definite scheme is
 298 particularly helpful for ecosystem model studies to eliminate negative tracer
 299 values associated purely with advection and diffusion.

300 The physical model is initialized from a resting state, and run with
 301 climatological surface and side-boundary forcing for a period of 6 years.
 302 The physical state following spinup is then combined with initial conditions
 303 for the ecosystem model to provide complete fields for the coupled physi-
 304 cal/ecosystem model. Initial conditions for nitrate, silicate, and phosphorous
 305 are taken from the winter season estimates of the 2005 World Ocean Atlas
 306 (<http://www.nodc.noaa.gov/OC5/WOA05/pubwoa05.html>). Initial condi-
 307 tions for all other fields are set to a very small value (10^{-5} $\mu\text{mole P l}^{-1}$ or
 308 a related value based on a Redfield ratio). Lateral boundary conditions for
 309 the ecosystem components are similar to the initial conditions, except that

the nitrate, phosphate and silicate values vary seasonally according to the seasonal average WOA05 fields. The coupled physical/ecosystem model is run with realistic forcing for 6 years duration from 1999 through 2004. The first year, 1999, is considered spinup of the ecosystem as it adjusts from its initial conditions to a more realistic state and is discarded from our analysis.

3. Results

3.1. Model Evaluation

Since the primary aim of this paper is to investigate biodiversity and biogeography in the CCS, it is important to quantitatively evaluate the model performance. Although we have no data to compare directly with biomass concentrations of individual modeled phytoplankton, we can evaluate the sum total of modeled phytoplankton biomass with satellite estimates. Chlorophyll estimates were obtained for years 2000 to 2004 from the monthly SeaWiFS Wide Field-of-View Sensor (SeaWiFS) products using the OC4V4 algorithm (O'Reilly et al., 1998) and were provided to us by NOAA Environmental Research Division. Data was reprocessed using a median smoothing algorithm and regridded to the same resolution as the model output.

Figure 3 shows $\log_{10}(\phi)$ where ϕ is the 5 year average chlorophyll from (a) the surface level of the numerical model or (b) the satellite derived data. The overall structure of the upwelling system is evident. In both panels, high biomass standing stock is found nearshore, the result of nutrient transport into the photic zone by coastal upwelling. The highest levels found in nature occur in the Gulf of the Farallones ($\sim 38^\circ\text{N}$), north of Cape Mendocino ($\sim 41^\circ\text{N}$), near Heceta Bank ($\sim 44^\circ\text{N}$), and the Washington coast ($\sim 46^\circ\text{N}$).

334 With the exception of the stock off Washington, modeled alongshore chloro-
335 phyll variation has a similar alongshore structure though at lower amplitude;
336 small local enhancements to the 5-year average concentration are found in
337 the model output in the Gulf of the Farallones, between Capes Mendocino
338 and Blanco, and a small increase near Heceta Bank. One reason for the
339 reduced amplitude in alongshore chlorophyll variation is the limited repre-
340 sentation of nearshore motions due to the model resolution and associated
341 topographic smoothing, common to all terrain-following coordinate models
342 (Haidvogel and Beckman, 1999). The high chlorophyll levels observed off
343 Washington and British Columbia have multiple causes, including nutrient
344 supply from the Straits of Juan de Fuca and Columbia river outflows (Hickey
345 and Banas, 2008), neither of which is included in the present model. Note-
346 worthy also in the visual comparison of Figure 3 is the chlorophyll reduction
347 in the southern California Bight. Though the depletion to the south is larger
348 in amplitude than found in nature, the model includes a small phytoplankton
349 increase in the Santa Barbara Channel just south of Pt. Conception as well
350 as a tongue extending to the southeast over the subsurface Santa Rosa Ridge
351 (topographic feature not shown).

352 The cross-shore breadth of the high chlorophyll zone is $O(100 \text{ km})$, similar
353 to the observations and other modeling studies (Plattner et al., 2005), though
354 the chlorophyll reduction with distance from coast is somewhat more rapid
355 in the model than in the nature. Offshore levels are consistently low, less
356 than about $0.3 \text{ mg chl m}^{-3}$ and consistent with more oligotrophic subtropical
357 gyre water. Modeled chlorophyll is too high in the southwestern portion of
358 the domain, likely the result of a numerical boundary influence.

359 We quantify model fidelity via a Taylor diagram, which graphically presents
 360 the correlation coefficient (CC), standard deviations normalized to that of
 361 the observations (NSD), and normalized, centered root mean squared error
 362 (RMSE) (Taylor, 2001). In this diagram, radial distance from the origin in-
 363 dicates NSD and the azimuthal direction represents CC, maximum of 1 along
 364 the x -axis. Truth in our analysis is defined by the observations and is repre-
 365 sented by the point in Figure 4a labeled SeaWiFS at a value of NSD=CC=1
 366 on the x -axis. The point labeled DOMAIN represents the statistical compar-
 367 ison of panels in Figure 3 and is found near the intersection of NSD=0.4 and
 368 CC=0.7. The high value for the correlation coefficient reflects the general
 369 agreement in overall structure of the near and offshore fields. To better under-
 370 stand the cause of the roughly one half reduction in variability, we decompose
 371 the domain into various subregions, similar to Gruber et al. (2006). North
 372 and South subdomains are divided by latitude 40.5°N , and coastal and off-
 373 shore regions are delineated by the 1000 m isobath. It is clear from the figure
 374 that the overall low standard deviation is dominated by the coastal region,
 375 related to alongshore variability nearshore discussed above. The southern
 376 offshore region has slightly lower NSD than the northern region, both rela-
 377 tive to their respective observations, and this low value likely results from the
 378 enhanced chlorophyll concentrations modeled in the southwest corner, also
 379 discussed above. All subregions exhibit correlation coefficients greater than
 380 0.5. Overall (data minus model) biases are also presented in the diagram
 381 as the number in parentheses near each point label. The domain average
 382 modeled field has an average bias (B) of $-0.13 \text{ mg chl m}^{-3}$, and this value
 383 represents a weighted average of the small value offshore ($B=-0.059 \text{ mg chl}$

384 m^{-3}) and the considerably larger bias in the coastal zone ($B=-1 \text{ mg chl m}^{-3}$).

385 The CCS seasonal cycle is reasonably represented as well (Figure 4b).
386 Seasons (winter, spring, summer, fall) are defined as collections of three calen-
387 dar months (JFM, AMJ, JAS, OND). All seasons have correlation coefficients
388 greater than 0.5, with the largest value ($CC=0.75$) occurring in springtime
389 (April-June). Spatial variability in chlorophyll is particularly low ($SD\sim 0.2$)
390 in Autumn (Oct-Dec) but approximately equal to the 5-year average vari-
391 ability in other seasons. Overall bias is low ($|B| < 0.26 \text{ mg chl m}^{-3}$) in all
392 seasons with the model usually under-predicting total chlorophyll biomass
393 (i.e., $B < 0$), as in the 5-year average.

394 *3.2. Surface Distributions*

395 With good correlation between total phytoplankton biomass modeled and
396 remotely sensed estimates in various parts of the domain, we now investigate
397 the magnitude and distributions of the phytoplankton that make up this
398 total. The 78 independent phytoplankton analogs initially seeded equally at
399 a low level ($10^{-5} \mu\text{mole P l}^{-1}$) and uniformly throughout the domain self-sort
400 themselves over time into a hierarchy that can be ordered by total biomass
401 contained within the full model volume. The 5-year average field reveals
402 38 phytoplankton existing at levels well above the baseline minimum level
403 maintained in the model for all fields. However, most of these members'
404 biomass are extremely small compared to the biomass of the top several
405 contributors. Eight primary producers that have concentrations exceeding
406 10% of the maximum, and six more maintain biomass between 0.3% and
407 1% of the maximum. Of these top eight phytoplankton, we find 2 diatoms,
408 1 LND, 3 PLP, and 2 SNP. In the next grouping of six are 2 diatoms, 2

409 LND, and 2 PLP. Thus all functional groups enabled are well represented
410 by the model at relatively substantial concentrations, and each consists of
411 further subtypes at various biomass levels. For simplicity, this manuscript
412 concentrates on total distributions for each functional group and the top
413 several subtypes.

414 Geographical distributions illustrate population horizontal structure. Shown
415 in Figure 5 are the 5-year average surface chlorophyll concentrations for di-
416 atoms, PLP, LND, and SNP (note the differing linear color-scale in each
417 panel). In the 5-year average, the total phytoplankton field is dominated
418 numerically by nearshore diatom concentrations. However, at considerably
419 lower but nonzero levels, LND are found more broadly, but at highest concen-
420 trations in the coastal transition zone between the upwelling and oligotrophic
421 offshore waters off central California. Also, PLP thrive well offshore of the
422 upwelling region, and SNP are distributed throughout the domain, though
423 with largest amplitudes both in the upwelling zone and in more oligotrophic
424 waters offshore.

425 It is possible to probe further into phytoplankton structure and biogeog-
426 raphy by examining the particular subtypes that constitute the functional
427 group totals. Figure 6 shows the top three PLP and two top SNP organisms
428 in terms of their total biomass. Multiple subtypes are supported within the
429 model, but they are not uniformly distributed. The top three PLP subtypes
430 have different temperature optima (approximately 11°, 17°, and 20°C), and
431 they thrive in middle, northern, and southern latitudes, respectively. Simi-
432 larly, the two dominant SNP are also distributed according to temperature
433 optima (16° and 10°C) and are found in the southern and northern portions

434 of the domain.

435 Surface distributions for grazers in the 5-year average are shown also in
436 Figure 5. Though found at greatest amplitude in the model in the southern
437 California Bight, microzooplankton are distributed over the full extent of the
438 CCS, supported by small and large phytoplankton available for consump-
439 tion throughout the domain. In contrast, large zooplankton have greatest
440 palatability for large phytoplankton and are found at highest intensity in
441 the upwelling zone, quickly dropping to vanishing levels as offshore distance
442 increases. Grazing of large on small zooplankton may also play an important
443 role governing these population distributions.

444 Over an annual cycle, phytoplankton biomass exhibits a strong seasonal
445 cycle (Figure 7) with well defined biogeographic patterns. As equatorward,
446 alongshore winds develop following the spring transition in March/April
447 (Strub et al., 1987), phytoplankton stocks increase nearshore within the
448 coastal upwelling zone. It is perhaps noteworthy that high coastal biomass is
449 found first to the south along the central and northern California coasts (be-
450 tween Pt. Conception at about 35°N and Cape Mendocino around 40°N), and
451 then to then north along the Oregon and Washington coasts as the upwelling
452 season progresses through August and September. With the weakening of
453 upwelling-favorable winds in fall (October through Dec), the CCS exhibits
454 relatively low phytoplankton levels over much of the domain. During late
455 winter/early spring (February - April), offshore northern waters undergo an
456 increase in phytoplankton levels, perhaps due to increased nutrients from
457 wintertime mixing and an increase in solar insolation.

458 3.3. Vertical Sections

459 Although the maps shown in the previous section provide context for
460 organisms that thrive at the surface, additional structure is found by exam-
461 ining subsurface concentrations. We illustrate the vertical structure along
462 a section (shown in Figure 3a) that overlays Line 67 of the California Co-
463 operative Oceanic Fisheries Investigations (www.calcofi.org) which extends
464 offshore in the cross-shore direction from Monterey Bay within the central
465 California coast. Although our model section extends hundreds of km further
466 than CalCOFI Line 67, we refer in this paper to this model transect as Line
467 67 for brevity. In the 5-year average (not shown), the vertical sections in
468 total phytoplankton and functional group fields reveal only surface maxima
469 that extend through a well-mixed region down 40 to 60 meters (shallower
470 values nearshore) followed by a gradient to vanishing levels between 90 and
471 140 m depth (deeper values nearshore). However, the annual cycle of the
472 sections reveal considerably more information. In Figure 8 are the monthly
473 sections for total modeled chlorophyll. From November through April phy-
474 toplankton structure is characterized by a well-mixed, near-surface field, de-
475 caying rapidly beneath. In March an upwelling-induced, nearshore bloom at
476 the surface appears and intensifies and persists through October. From May
477 through October, a broad subsurface chlorophyll maximum develops offshore
478 of the upwelling region. This offshore maximum is found around 70 m depth,
479 at the top of the modeled nutricline and within the thermocline beneath a
480 seasonally warmed surface layer (not shown).

481 Analysis of the individual functional group fields indicates that this sub-
482 surface phytoplankton maximum results primarily from diatoms and SNP

483 which occur at much lower levels in the offshore surface waters at these
 484 times of the year. The PLP group also contributes to the phytoplankton to-
 485 tal at depth but has significant concentrations above this deep maximum, and
 486 therefore this group is not itself responsible for its existence. LND are found
 487 mostly above the deep maximum. Although the PLP group has a broad pres-
 488 ence extending from the surface to the top of the nutricline, subtypes within
 489 this group reveal strata. Shown in Figure 9 are the 5-year averaged July
 490 and August fields for the top two PLP. These two subtypes occupy different
 491 niches within the water column. PLP #1 ($k_{par}=0.01 \text{ W}^{-1} \text{ m}^2$) is adapted to
 492 high light conditions and is found near the surface in both months whereas
 493 #2 ($k_{par}=0.026 \text{ W}^{-1} \text{ m}^2$) is more likely to thrive in subsurface waters with
 494 low PAR levels and is found at depth.

495 3.4. Temporal Succession

496 The sequence of plankton populations within the modeled CCS is esti-
 497 mated by integrating the surface biomass distributions horizontally over the
 498 domain. Figure 10 plots time-series for total phytoplankton and individ-
 499 ual functional groups. All fields show clear seasonal cycles, but the timing
 500 of individual functional group maxima varies. The total phytoplankton field
 501 (panel a, blue) reveals a late springtime peak and is dominated by the diatom
 502 population (panel b, blue). However, while the diatom population declines
 503 to small or near zero levels during fall and winter, the total phytoplankton
 504 biomass within the CCS maintains a low level, but well above zero, and ev-
 505 idently supported by non-diatom fields. The small phytoplankton biomass
 506 (panel a, green) shows smaller amplitude variation than the total, with max-
 507 imum in early spring. This more limited seasonal cycle results from two

508 out-of-phase oscillations; SNP (panel c, green) exhibits a wintertime increase
509 preceding the growth in and extending longer than the diatom population.
510 In contrast, PLP (panel c, blue) reaches its nadir in spring and maximum in
511 fall. LND (panel b, green) exhibit 2 peaks annually, with a maximum in the
512 spring but after the diatoms, and then a subsequent, larger increase in late
513 summer, early fall that is quite out of phase with the diatom cycle.

514 For completeness, we present the grazer fields, although given the complex
515 spatial structure of the primary and secondary producers discussed above,
516 we caution about over-interpreting the biomass pathways within the model
517 from this simplistic representation. Like the phytoplankton, the zooplankton
518 fields also display seasonal cycles. Microzooplankton (panel d, blue) levels
519 fluctuate similar to, though slightly later than, the PLP distribution. The
520 microzooplankton fields grow in late summer/autumn, but it is important to
521 note that their minimum levels are not close to zero. Rather, they sustain
522 a nonzero integrated biomass and thus nonzero grazing pressure throughout
523 the year. Mesozooplankton (panel d, green) begin to develop early in the year
524 at the same time as diatoms, but they reach their maximum well after the
525 diatom peak, near the same time as the LND group. The large zooplankton
526 approach very small levels in winter, unlike the offseason for small grazers.

527 As with the surface maps, each functional group can be further inspected
528 for subtypes. Figure 11 shows the top few subtypes for diatoms, LND, SNP,
529 and PLP in panels a, b, c, and d, respectively. Whereas big phytoplankton
530 are dominated by single subtypes, the small phytoplankton can be divided
531 into multiple non-negligible components whose timing for growth and decline
532 are shifted and apparently unrelated. It is perhaps surprising that the spring

533 and fall increases in LND result from only one subtype, but it argues that for
534 some organisms, environmental conditions for which they are best adapted
535 can arise at multiple times in the year, and not simply once in an annual
536 cycle.

537 4. Discussion

538 The goal of this study is to evaluate the emergent community ecosys-
539 tem model for its capacity to represent the biodiversity and biogeography
540 of the California Current System. Observations have long shown diverse,
541 heterogeneous planktonic communities, though usually with single or a few
542 species numerically dominant. Studies based on phytoplankton counts fo-
543 cused on larger taxa. The Balech (1960) study of coastal waters off Scripps
544 pier in Southern California documented both diatoms and dinoflagellates,
545 with diatoms being most abundant but dinoflagellates comprising half the
546 listed phytoplankton. Bolin and Abbott (1963) reported that while one genus
547 (*Chaetoceros* spp.) appeared most numerous in the large-sized phytoplank-
548 ton population in Monterey Bay between 1954 and 1960, 17 other genera
549 were observed at lower levels. More broadly, Venrick (2009) identified 294
550 taxa of phytoplankton along Line 87 from the CalCOFI sampling grid off
551 southern California. The most abundant were a centric diatom (*Chaeto-*
552 *ceros debilis*), a coccolithophorid (*Emilinia huxleyi*) and a pennate diatom
553 (robust *Pseudo-nitzschia*). Together, these three species accounted for 61%
554 of the total abundance, and thus the numerical contribution of most of the
555 remaining 291 taxa to the total is extremely small. More modern techniques
556 have revealed extensive picophytoplankton abundance further contributing

557 to this biodiversity. Flow cytometer analysis and epifluorescence microscopy
558 have documented the presence of *Synechococcus* and picoeukaryotes, and to
559 a lesser extent *Prochlorococcus*, in different coastal domains off Oregon and
560 California (Hood et al., 1991; Collier and Palenik, 2003; Worden et al., 2004;
561 Sherr et al., 2005).

562 Overall, the model output analyzed in this manuscript represents this ob-
563 served phytoplankton biodiversity. Of 78 phytoplankton types seeded in the
564 model, approximately 40 coexist in the multi-year average. The top 14 or-
565 ganisms in terms of area averaged surface biomass span 3 orders of magnitude
566 in that measure; they include 4 diatoms, 3 large non-diatoms (a group which
567 would include dinoflagellates), 5 *Prochlorococcus*-like organisms, and 2 small
568 phytoplankton that can use nitrate (which would include *Synechococcus* and
569 picoeukaryotes). Although the breadth of organisms and functional groups
570 is not as extensive as that in nature, it represents a significant advance over
571 existing ecosystem models that characterize the phytoplankton community
572 with only one or two components.

573 The model biogeography also shows considerable promise when compared
574 to observations. We quantitatively evaluated the total modeled chlorophyll
575 against SeaWiFS-derived surface chlorophyll estimates on a 5-year and sea-
576 sonal mean basis. The model shows good representation of the general pat-
577 tern of standing stock in the California Current System ($0.5 < CC < 0.75$) for
578 the years 2000-2004. The standard deviation of total chlorophyll is approx-
579 imately one half that observed in nature. In part we believe, this low vari-
580 ability results from limited (~ 10 km) physical model resolution, and though
581 not shown in this paper, this measure can be adjusted also through some

parameter tuning, such as of the carbon to chlorophyll ratio. Noteworthy peaks and deficits of surface chlorophyll are found along the coast at multiple locations in both model and observations. The most widely-recognized biogeographic boundary in the California Current System occurs in nature at Pt. Conception (Checkley and Barth, 2009). In our model, this break is visible in both the total surface phytoplankton stock (Figure 3) and in the surface diatom field (Figure 5a). It is perhaps a failing of the model that this break is not clearly visible at the next higher trophic level (Figure 5e and f). However, our effort has focused on phytoplankton diversity, and it may be that greater resolution of the zooplankton community and/or explicit temperature dependence on grazing or metabolic rate may be necessary.

The general horizontal structure of the modeled functional groups also appears reasonable, though our ability to quantitatively evaluate this aspect is not as great as with the total phytoplankton stock. It is well known that high nutrient input resulting from coastal upwelling in the CCS drives new production of nearshore diatom blooms (Barber and Smith, 1981), with considerably smaller diatom abundance found in oligotrophic waters. Because many ecosystem models only parameterize in terms of diatoms, the cross-shore diatom structure is common to other, single functional group models (e.g., Gruber et al., 2006) and also idealized studies (Spitz et al., 2003; Edwards et al., 2000a). Less common is the representation of *Prochlorococcus* (our PLP group) and *Synechococcus* or picoeukaryotes (our SNP group). In our multi-year average, we find an increase in our SNP group close to the coast and offshore, with a smaller but still significant presence all through the domain. PLP shows a distinct deficit in the nearshore upwelling zone with

607 increasing concentration westward and to the south in more oligotrophic wa-
608 ters (Figure 5).

609 We believe that this general small phytoplankton structure is consistent
610 with observations. Worden et al. (2004) found off the Scripps pier in southern
611 California that *Synechococcus* dominated cell abundance and picoeukary-
612 otes contributed most to estimated carbon biomass. Along a transect off
613 Oregon, Sherr et al. (2005) found small-sized phytoplankton dominated by
614 *Synechococcus* and picoeukaryotes at near shore stations just offshore of the
615 upwelling front. Collier and Palenik (2003) identified a gradient in *Syne-*
616 *chococcus* abundance across the CalCOFI sampling grid, with highest levels
617 nearshore of the California Current and lower levels offshore. *Prochlorococcus*
618 shows the opposite tendency. Worden et al. (2004) report that *Prochloro-*
619 *coccus* were small contributors to total biomass and sometimes not found
620 at all at their coastal station. Sherr et al. (2005) observed *Prochlorococcus*
621 only at one offshore station in their sampling grid. In contrast, at Station
622 ALOHA in the North Pacific Subtropical Gyre, *Prochlorococcus* has been
623 found to contribute about 40% or more of the total photosynthetic biomass
624 (Campbell et al., 1994).

625 A last aspect of the CCS biogeography that the model appears to capture
626 is in the vertical. In the Sherr et al. (2005) study, *Synechococcus* was often
627 found to be nearly coincident with picoeukaryotes, but at some cross-shore
628 sections, notably July 2002, *Synechococcus* occupied surface waters, and pi-
629 coeukaryotes exhibited a clear subsurface maximum. Although reported for
630 the years 1997-1998 which were complicated by El Niño and La Niña events,
631 Chavez et al. (2002) present chlorophyll distributions along Line 67 which

632 in 1999 (the La Niña year) show subsurface chlorophyll maximum 200-300
633 km offshore from February through October. This feature was also noted in
634 the modeling study of Gruber et al. (2006) along nearby CalCOFI Line 70
635 to the south. In our model, subsurface chlorophyll maxima are found along
636 CalCOFI line 67 in the 5-year average fields from May to October. We find
637 this maximum is composed of diatoms and SNP. In addition, we find a divi-
638 sion within the *Prochlorococcus*-like organisms. Highest total concentrations
639 are found at the surface, though subtypes with low-light adaptations occupy-
640 ing subsurface strata. These broad descriptions are similar to those outlined
641 from observations along the Atlantic Meridional Transect by Johnson et al.
642 (2006) and have been observed and modeled at Station ALOHA (Rabouille
643 et al., 2007).

644 Finally, within this paper we have investigated phytoplankton succession
645 in the CCS. Within Monterey Bay in 1976 and 1977, Garrison (1979) ob-
646 served communities in which diatoms dominated from winter through the
647 upwelling period and dinoflagellate occasionally becoming more abundant
648 in the fall. Chavez et al. (2002) suggest that nearshore central California
649 coastal waters transition from diatom dominated upwelling system to a pi-
650 coplankton community in the so-called oceanic (fall) period. We find diatoms
651 exhibit the largest chlorophyll concentrations in the multi-year average, but
652 that their amplitudes are highly variable in time. Strongest diatom levels oc-
653 cur in the spring/summer period (Figure 11), and large phytoplankton that
654 does not require silicate peaks in late summer/early fall during the diatom
655 minimum. Small phytoplankton also experience strong seasonal cycles, with
656 our PLP and SNP largely out of phase with one another; we find a fall peak

657 in *Prochlorococcus*-like organisms and a spring minimum.

658 The results presented in this paper describe only one realization of this
659 ecosystem model. One distinguishing feature of the present approach is the
660 method of parameter selection. Although, as in more traditional models,
661 many important constants in this model are chosen by the operator, a few
662 key parameters that govern phytoplankton growth are selected randomly
663 within reasonable ranges. Different realizations of the random numbers will
664 yield different subsets of virtual phytoplankton, allowing for potentially very
665 different autotrophic communities. While our main realization described in
666 this manuscript consists of 5 years of model output, we have also investi-
667 gated other randomizations for a shorter duration. Figure 12 presents the
668 Taylor diagram comparing total phytoplankton at the surface from 5 ecosys-
669 tem realizations to SeaWiFS chlorophyll estimates for the year 2000 (one
670 year following ecosystem spinup). Number 1 corresponds to the run de-
671 scribed throughout this paper. It is evident that all ecosystem realizations
672 have similar domain-wide correlation coefficients ($0.6 < CC < 0.7$). Greater
673 scatter is found in the radial direction, and run 3 has the largest NSD, and
674 the point closest to the SeaWiFS estimate. All runs also have very similar
675 biases. Thus changing the modeled phytoplankton through random physio-
676 logical responses gives very robust model output in terms of total, averaged
677 phytoplankton biomass.

678 What does vary in different realizations is the underlying number and
679 detailed distribution of significant functional group subtypes that emerge.
680 Within each realization, all four functional groups have members that ex-
681 ist at levels exceed 10% of the maximum biomass. Most consistent among

682 realizations is (a) the existence of one, two, or three coastal diatoms of sig-
683 nificant biomass, (b) the offshore presence of PLP, and (c) the occurrence
684 of SNP both on and offshore. LND are the most variable functional group
685 across realizations, with representatives that inhabit the coastal transition
686 zone/offshore regions (runs 2 and 4), the coastal domain (run 3) or both
687 (runs 1 and 5).

688 Although typical of many ecosystem models in which some biological pro-
689 cesses are better represented or parameterized than others, it is important to
690 note some of the model shortcomings. Large non-diatoms are a group defined
691 in this model that, within the California Current System, arguably represents
692 flagellates and dinoflagellates. Evidence supports these organisms attaining
693 resources in more complex ways than typical of other phytoplankton, such
694 as through mixotrophy, vertical migration, and assimilation of nitrogen in
695 the dark (Harrison, 1976), which are not included in the model. Although
696 zooplankton populations have been shown to play a large role in shaping the
697 structure of the phytoplankton community (Verity and Smetacek, 1996), and
698 species-specific preferences of zooplankton on phytoplankton have been re-
699 ported (e.g., Cowles et al., 1988; Flynn et al., 1996) we maintained relatively
700 simple zooplankton representation with only one large and one small member.
701 While Redfield ratios enable a compact representation that is computa-
702 tionally efficient for ecosystem models, considerable evidence reveals interesting
703 deviations from these quantities under periods of nutrient stress (Geider and
704 La Roche, 2002). In the present model, phytoplankton are assumed to be
705 in Redfield proportions. Quantitative model evaluation was aided by vari-
706 able, group-specific carbon to chlorophyll ratio. It is possible that a more

707 complex representation of carbon to chlorophyll may further aid in this as-
708 sessment, particularly with depth distributions. Finally, we have neglected
709 the influence of iron as a limiting micronutrient in the model. Evidence (e.g.,
710 Hutchins and Bruland, 1998; Bruland et al., 2001) has shown the possibility
711 for iron limitation within the coastal waters of the California Current System,
712 and this model capability remains to be explored.

713 Thus, the neglect of some phytoplankton behavior, limited grazer di-
714 versity, assumed Redfield stoichiometry for phytoplankton, fixed carbon to
715 chlorophyll ratios, and the omission of iron as a limiting resource are all as-
716 pects of the model that could be improved upon. However, despite these
717 shortcomings, this model does an excellent job of representing many aspects
718 of the California Current Ecosystem and offers for the first time in this re-
719 gion substantial biodiversity of modeled organisms with temporal and spatial
720 structure that should further illuminate role of physical and biological pro-
721 cesses that govern these populations.

722 **5. Acknowledgements**

723 We are grateful to the Gordon and Betty Moore Foundation for grants
724 supporting this research. Thanks to Jim Doyle for help with COAMPS and to
725 Patrick Heimbach for assistance with the ECCO product. The work was im-
726 proved through valuable conversations with Jerome Fiechter, Andy Leising,
727 Sophie Rabouille, Francisco Chavez, and Stephanie Dutkiewicz. SeaWiFS
728 data provided by NOAA, Pacific Fisheries Environmental Laboratory, cour-
729 tesy of NASA Goddard Space Flight Center, Ocean Biology Products Group
730 and Geoeye, Inc.

731 Appendix A.

732 This appendix documents the equations used in the ecosystem model,
 733 shown schematically in Figure 1. Constants used in the formulation are
 734 given in Tables A.1, A.2, and A.3. Using words to represent processes, the
 735 rates of change of model state variables can be expressed

$$\begin{aligned}
 \frac{\partial \text{phytoplankton}}{\partial t} &= \text{uptake} - \text{grazing} - \text{phytoplankton mortality} \\
 \frac{\partial \text{zooplankton}}{\partial t} &= \text{assimilated grazing} - \text{zooplankton mortality} \\
 \frac{\partial \text{nutrients}}{\partial t} &= \text{remineralization} - \text{uptake} \\
 \frac{\partial \text{particulates}}{\partial t} &= \text{export to particulates} - \text{particulate remineralization} - \text{sinking} \\
 \frac{\partial \text{dissolved organics}}{\partial t} &= \text{export to dissolved} - \text{dissolved remineralization}.
 \end{aligned}$$

736 It is convenient to describe each processes individually and consider sep-
 737 arately the associated rate of change for each state variable. The model
 738 includes N_p phytoplankton members and N_z zooplankton organisms. We use
 739 subscripts, i , j , and k to identify individual phytoplankton or zooplankton
 740 but omit these indices when the context is clear. All state variables, which
 741 are concentrations and denoted with square brackets, are functions of space
 742 and time, (e.g.,

$$[P_i] = [P_i](x, y, z, t) \tag{A.1}$$

743 for phytoplankton i) though we omit reference to these dependencies except
 744 when necessary for clarity.

745 For each phytoplankton, i , growth by nutrient uptake is given by

$$U_i = \mu_i I_{lim} N_{lim} T_{lim} [P_i] \quad (\text{A.2})$$

746 where μ_i is the maximum growth rate. Growth is reduced from its maximum
747 value by three factors, I_{lim} , N_{lim} , and T_{lim} , representing limitation by light,
748 nutrients, and temperature, respectively.

749 The light function is expressed

$$I_{lim} = \frac{1}{\gamma} (1 - e^{-k_{par} I_{PAR}}) e^{-k_{inh} I_{PAR}} \quad (\text{A.3})$$

$$\gamma = \frac{k_{par}}{k_{par} + k_{inh}} \ln\left(\frac{k_{inh}}{k_{par} + k_{inh}}\right). \quad (\text{A.4})$$

750 Here, I_{PAR} is the local photosynthetically active radiation, which depends
751 on the surface PAR, I_s , and subsurface total phytoplankton concentration:

$$I_{PAR}(z) = I_s e^{-\int_z^0 (k_0 + k_p P_T(z)) dz} \quad (\text{A.5})$$

752 and

$$P_T(z) = \sum_{i=0}^{N_p} [P_i](z). \quad (\text{A.6})$$

753 Parameters k_{inh} and k_{par} are phytoplankton-dependent,

$$k_{par} = |\mathcal{N}(\overline{k_{par}}, \sigma_{k_{par}})| \quad (\text{A.7})$$

$$k_{inh} = |\mathcal{N}(\overline{k_{inh}}, \sigma_{k_{inh}})| \quad (\text{A.8})$$

754 where $\mathcal{N}(\overline{\nu}, \sigma_\nu)$ is a normal random deviate with mean, $\overline{\nu}$, and standard
755 deviation, σ_ν . Values for the means and standard deviations of these light
756 parameters are provided in Table A.1.

757 Limitation by temperature, T , is given by

$$T_{lim} = c_a(c_b^T e^{-\left(\frac{|T-T_O|}{T_d}\right)^\tau} - T_n) \quad (A.9)$$

$$(A.10)$$

758 where

$$T_O = \mathcal{U}(T_{min}, T_{max}) \quad (A.11)$$

759 is the temperature optimum, and $\mathcal{U}(\nu_0, \nu_1)$ is a uniform random deviate be-
760 tween ν_0 and ν_1 .

761 Nutrient limitation is determined as the minimum of multiple nutrient
762 limitation functions, the choice of which depends on the silicate requirement
763 and the forms of nitrogen utilized. For phytoplankton that require silicate
764 and process all three forms of nitrogen,

$$L_P = \frac{[PO_4]}{k_{PO_4} + [PO_4]} \quad (A.12)$$

$$L_{Si} = \frac{[Si(OH)_4]}{k_{Si} + [Si(OH)_4]} \quad (A.13)$$

$$L_{NH_4} = \frac{[NH_4]}{k_{NH_4} + [NH_4]} \quad (A.14)$$

$$L_{NO_2} = \frac{[NO_2]}{k_{NO_3} + [NO_2] + [NO_3]} e^{-\sigma_A[NH_4]} \quad (A.15)$$

$$L_{NO_3} = \frac{[NO_3]}{k_{NO_3} + [NO_2] + [NO_3]} e^{-\sigma_A([NH_4])} \quad (A.16)$$

$$L_N = L_{NH_4} + L_{NO_2} + L_{NO_3}. \quad (A.17)$$

765 For phytoplankton that do not use silicate but assimilate ammonium and

766 nitrite, we set

$$L_P = \frac{[PO_4]}{k_{PO_4} + [PO_4]} \quad (A.18)$$

$$L_{NH_4} = \frac{[NH_4]}{k_{NH_4} + [NH_4]} \quad (A.19)$$

$$L_{NO_2} = \frac{[NO_2]}{k_{NO_2} + [NO_2]} e^{-\sigma_A [NH_4]} \quad (A.20)$$

$$L_N = L_{NH_4} + L_{NO_2}. \quad (A.21)$$

767 For autotrophs that do not use silicate and take up ammonium only,

$$L_P = \frac{[PO_4]}{k_{PO_4} + [PO_4]} \quad (A.22)$$

$$L_{NH_4} = \frac{[NH_4]}{k_{NH_4} + [NH_4]} \quad (A.23)$$

$$L_N = L_{NH_4}. \quad (A.24)$$

768 Half saturation constants for nutrient uptake are assigned as uniform random
 769 deviates between bounds given in Table A.1. Finally, the nutrient limitation
 770 factor is defined

$$N_{lim} = \begin{cases} \min(L_P, L_{Si}, L_N) & \text{diatom} \\ \min(L_P, L_N) & \text{otherwise} \end{cases}. \quad (A.25)$$

771 The rate of change of phytoplankton biomass and nutrients due to growth

772 by a single phytoplankter is expressed

$$\frac{\partial[P_i]}{\partial t} = U_i \quad (\text{A.26})$$

$$\frac{\partial[PO_4]}{\partial t} = -U_i \quad (\text{A.27})$$

$$\frac{\partial[Si(OH)_4]}{\partial t} = \delta_{Si} r_{SiP} \frac{\partial[PO_4]}{\partial t} \quad (\text{A.28})$$

$$\frac{\partial[NO_3]}{\partial t} = f_{NO3} r_{NP} \frac{\partial[PO_4]}{\partial t} \quad (\text{A.29})$$

$$\frac{\partial[NO_2]}{\partial t} = f_{NO2} r_{NP} \frac{\partial[PO_4]}{\partial t} \quad (\text{A.30})$$

$$\frac{\partial[NH_4]}{\partial t} = f_{NH4} r_{NP} \frac{\partial[PO_4]}{\partial t}. \quad (\text{A.31})$$

773 in which the variable δ_{Si} takes on a value of 1 if silica is required and 0 when
 774 it is not, and factors r_{SiP} , etc., are Redfield ratios. Using the δ notation also
 775 for nitrogen utilization, we define the factors that partition nitrogen uptake
 776 to depend on both this ability to use a particular form and the relative
 777 availability of that resource:

$$f_{NO3} = \delta_{NO3} \frac{L_{NO3}}{L_N} \quad (\text{A.32})$$

$$f_{NO2} = \delta_{NO2} \frac{L_{NO2}}{L_N} \quad (\text{A.33})$$

$$f_{NH4} = \delta_{NH4} \frac{L_{NH4}}{L_N}. \quad (\text{A.34})$$

778 For grazing, we consider processes influenced by zooplankton k . Total
 779 grazable material for zooplankton k , weighted by its palatability, is given by

$$A_k = \sum_{i=0}^{N_p} \pi_{ki}^{(P)} [P_i] + \sum_{j=1}^{N_z} \pi_{kj}^{(Z)} [Z_j] \quad (\text{A.35})$$

780 where $\pi_{ki}^{(P)}$ and $\pi_{kj}^{(Z)}$ represent the palatability of phytoplankton i and zoo-
 781 plankton j for grazer k . The rate for grazing of zooplankton j by zooplankton

782 k is given by

$$G_{kj}^{(Z)} = \frac{G_k^{max} \pi_{kj}^{(Z)} [Z_j] A_k}{k_g^2 + A_k^2} \quad (\text{A.36})$$

783 which then gives the rates of change for zooplankton biomass and particulate
784 and dissolved concentrations by grazing of organism j by k :

$$\frac{\partial [Z_j]}{\partial t} = -G_{kj}^{(Z)} [Z_k] \quad (\text{A.37})$$

$$\frac{\partial [Z_k]}{\partial t} = \alpha_k^{(Z)} G_{kj}^{(Z)} [Z_k] \quad (\text{A.38})$$

$$\frac{\partial [POP]}{\partial t} = E^{(G)} (1 - \alpha_k^{(Z)}) G_{kj}^{(Z)} [Z_k] \quad (\text{A.39})$$

$$\frac{\partial [DOP]}{\partial t} = (1 - E^{(G)}) (1 - \alpha_k^{(Z)}) G_{kj}^{(Z)} [Z_k]. \quad (\text{A.40})$$

785 The parameters $\alpha^{(Z)}$ and $E^{(G)}$ represent the assimilation efficiency and frac-
786 tion exported to particulate matter, respectively.

787 Analogously, the grazing rate for zooplankton k on phytoplankton i is
788 given by

$$G_{ki}^{(P)} = \frac{G_k^{max} \pi_{ki}^{(P)} [P_i] A_k}{k_g^2 + A_k^2} \quad (\text{A.41})$$

789 which yields for each component

$$\frac{\partial [P_i]}{\partial t} = -G_{ki}^{(P)} [Z_k] \quad (\text{A.42})$$

$$\frac{\partial [Z_k]}{\partial t} = \alpha_k^{(P)} G_{ki}^{(P)} [Z_k] \quad (\text{A.43})$$

$$\frac{\partial [POP]}{\partial t} = E^{(G)} (1 - \alpha_k^{(P)}) G_{ki}^{(P)} [Z_k] \quad (\text{A.44})$$

$$\frac{\partial [DOP]}{\partial t} = (1 - E^{(G)}) (1 - \alpha_k^{(P)}) G_{ki}^{(P)} [Z_k]. \quad (\text{A.45})$$

790 Mortality of phytoplankton and zooplankton induce changes in biomass

791 and dissolved and particulate compartments,

$$\frac{\partial[P_i]}{\partial t} = -m^{(P)} [P_i] \quad (\text{A.46})$$

$$\frac{\partial[Z_j]}{\partial t} = -m^{(Z)} [Z_j] \quad (\text{A.47})$$

$$\frac{\partial[POP]}{\partial t} = E^{(P)} m^{(P)} [P_i] + E^{(Z)} m^{(Z)} [Z_j] \quad (\text{A.48})$$

$$\frac{\partial[DOP]}{\partial t} = (1 - E^{(P)}) m^{(P)} [P_i] + (1 - E^{(Z)}) m^{(Z)} [Z_j]. \quad (\text{A.49})$$

792 Remineralization processes also influence these pools. For phosphorous,

$$\frac{\partial[POP]}{\partial t} = -k_{pop} [POP] \quad (\text{A.50})$$

$$\frac{\partial[DOP]}{\partial t} = -k_{dop} [DOP] \quad (\text{A.51})$$

$$\frac{\partial[PO_4]}{\partial t} = k_{dop} [DOP] + k_{pop} [POP]. \quad (\text{A.52})$$

793 For nitrogen,

$$\frac{\partial[PON]}{\partial t} = -k_{pon} [PON] \quad (\text{A.53})$$

$$\frac{\partial[DON]}{\partial t} = -k_{don} [DON] \quad (\text{A.54})$$

$$\frac{\partial[NH_4]}{\partial t} = k_{don} [DON] + k_{pon} [PON]. \quad (\text{A.55})$$

794 And for silica and silicate,

$$\frac{\partial[PSi]}{\partial t} = -k_{psi} [PSi] \quad (\text{A.56})$$

$$\frac{\partial[Si(OH)_4]}{\partial t} = k_{psi} [PSi]. \quad (\text{A.57})$$

795 For nitrification, we define the light function,

$$\mathcal{I} = \begin{cases} 1 - \frac{I_{PAR}}{I_0} & I_{PAR} \leq I_0 \\ 0 & I_{PAR} > I_0 \end{cases} \quad (\text{A.58})$$

796 which takes a value of 1 during darkness and 0 when PAR exceeds a critical
 797 value. Then

$$\frac{\partial[NH_4]}{\partial t} = -\mathcal{I} k_A [NH_4] \quad (\text{A.59})$$

$$\frac{\partial[NO_2]}{\partial t} = \mathcal{I} (k_A [NH_4] - k_B [NO_2]) \quad (\text{A.60})$$

$$\frac{\partial[NO_3]}{\partial t} = \mathcal{I} k_B [NO_2]. \quad (\text{A.61})$$

798 Finally, sinking obeys the following relations:

$$\frac{\partial[P_i]}{\partial t} = -w_p \frac{\partial[P_i]}{\partial z} \quad (\text{A.62})$$

$$\frac{\partial[POP]}{\partial t} = -w_{pom} \frac{\partial[POP]}{\partial z} \quad (\text{A.63})$$

$$\frac{\partial[PON]}{\partial t} = -w_{pom} \frac{\partial[PON]}{\partial z} \quad (\text{A.64})$$

$$\frac{\partial[PSi]}{\partial t} = -w_{pom} \frac{\partial[PSi]}{\partial z}. \quad (\text{A.65})$$

References

- Balech, E., 1960. The changes in the phytoplankton population off the California coast. In: The changing Pacific ocean in 1957 and 1958. Calif. Coop. Oceanic Fish. Invest. Rep. 7, 127–132.
- Banas, N. S., Lessard, E. J., Kudela, R. M., MacCready, P., Peterson, T. D., Hickey, B. M., Frame, E., 2009. Planktonic growth and grazing in the Columbia River plume region: A biophysical model study. J. Geophys. Res. C 114.
- Barber, R. T., Smith, R. L., 1981. Coastal upwelling ecosystems. Academic Press, Ch. 2, p. 3168.
- Bolin, R. L., Abbott, D. P., 1963. Studies on the marine climate and phytoplankton of the central coastal area of California, 1954-1960. Calif. Coop. Oceanic Fish. Invest. Rep. 9, 23–45.
- Brand, L. E., 1981. Genetic-variability in reproduction rates in marine-phytoplankton populations. Evolution 35 (6), 1117–1127.
- Brand, L. E., Guillard, R. R. L., 1981. The effects of continuous light and light-intensity on the reproduction rates of 22 species of marine phytoplankton. J. Exp. Mar. Biol. Ecol. 50 (2-3), 119–132.
- Broquet, G., Edwards, C. A., Moore, A. M., Powell, B. S., Veneziani, M., Doyle, J. D., 2009. Application of 4D-Variational Data Assimilation to the California Current System. Dyn. Atm. Oceans 48 (1-3), 69–92.

- 820 Bruland, K. W., Rue, E. L., Smith, G. J., 2001. Iron and macronutrients
821 in California coastal upwelling regimes: Implications for diatom blooms.
822 Limnol. Oceanogr. 46 (7), 1661–1674.
- 823 Brush, M. J., Brawley, J. W., Nixon, S. W., Kremer, J. N., 2002. Model-
824 ing phytoplankton production: problems with the Eppley curve and an
825 empirical alternative. Mar. Ecol. Prog. Ser. 238, 31–45.
- 826 Buck, K. R., Chavez, F. P., Campbell, L., 1996. Basin-wide distributions of
827 living carbon components and the inverted trophic pyramid of the central
828 gyre of the North Atlantic Ocean, summer 1993. Aquat. Microb. Ecol.
829 10 (3), 283–298.
- 830 Campbell, L., Nolla, H. A., Vault, D., 1994. The importance of *Prochlorococ-*
831 *cus* to community structure in the central North Pacific. Limnol. Oceanogr.
832 39, 954–961.
- 833 Chai, F., Dugdale, R. C., Peng, T. H., Wilkerson, F. P., Barber, R. T.,
834 2002. One-dimensional ecosystem model of the equatorial Pacific upwelling
835 system. Part I: Model development and silicon and nitrogen cycle. Deep-
836 Sea Res. II 49 (13-14), 2713–2745.
- 837 Chan, A. T., 1978. Comparative physiological study of marine diatoms and
838 dinoflagellates in relation to irradiance and cell-size. 1. Growth under con-
839 tinuous light. J. Phycol. 14 (4), 396–402.
- 840 Chan, A. T., 1980. Comparative physiological study of marine diatoms and
841 dinoflagellates in relation to irradiance and cell-size. 2. Relationship be-

842 tween photosynthesis, growth, and carbon-chlorophyll a-ratio. *J. Phycol.*
843 16 (3), 428–432.

844 Chang, J., Shiah, F. K., Gong, G. C., Chiang, K. P., 2003. Cross-shelf varia-
845 tion in carbon-to-chlorophyll a ratios in the East China Sea, summer 1998.
846 *Deep-Sea Res. II* 50 (6-7), 1237–1247.

847 Chavez, F. P., Buck, K. R., Service, S. K., Newton, J., Barber, R. T., 1996.
848 Phytoplankton variability in the central and eastern tropical Pacific. *Deep-*
849 *Sea Res. II* 43 (4-6), 835–870.

850 Chavez, F. P., Pennington, J. T., Castro, C. G., Ryan, J. P., Michisaki, R. P.,
851 Schlining, B., Walz, P., Buck, K. R., McFadyen, A., Collins, C. A., 2002.
852 Biological and chemical consequences of the 1997-1998 El Niño in central
853 California waters. *Prog. Oceanogr.* 54 (1-4), 205–232.

854 Checkley, Jr., D. M., Barth, J. A., 2009. Patterns and processes in the Cali-
855 fornia Current System. *Prog. Oceanogr.*

856 Collier, J. L., Palenik, B., 2003. Phycoerythrin-containing picoplankton in
857 the Southern California Bight. *Deep-Sea Res. II* 50, 2405–2422.

858 Conway, H. L., 1977. Interactions of inorganic nitrogen in uptake and assim-
859 ilation by marine-phytoplankton. *Marine Biology* 39 (3), 221–232.

860 Cowles, T. J., Olson, R. J., Chisholm, S. W., 1988. Food selection by cope-
861 pods: discrimination on the basis of food quality. *Marine Biology* 100 (1),
862 41–49.

- 863 Dugdale, R. C., Goering, J. J., 1967. Uptake of new and regenerated forms
864 of nitrogen in primary productivity. *Limnol. Oceanogr.* 12, 196–206.
- 865 Edwards, C. A., Batchelder, H. P., Powell, T. M., 2000a. Modeling micro-
866 zooplankton and macrozooplankton dynamics within a coastal upwelling
867 system. *J. Plankton Research* 22, 1619–1648.
- 868 Edwards, C. A., Powell, T. A., Batchelder, H. P., 2000b. The stability of
869 an NPZ model subject to realistic levels of vertical mixing. *J. Mar. Res.*
870 58 (1), 37–60.
- 871 Eppley, R. W., 1972. Temperature and phytoplankton growth in the sea.
872 *Fish Bull* 70 (4), 1063–1085.
- 873 Eppley, R. W., Coatsworth, J. L., Solorzano, L., 1969. Studies of nitrate
874 reductase in marine phytoplankton. *Limnol. Oceanogr.* 14, 194–205.
- 875 Fasham, M. J. R., Ducklow, H. W., McKelvie, S. M., 1990. A nitrogen-based
876 model of plankton dynamics in the oceanic mixed layer. *J. Mar. Res.* 48,
877 591–639.
- 878 Finkel, Z. V., 2001. Light absorption and size scaling of light-limited
879 metabolism in marine diatoms. *Limnol. Oceanogr.* 46 (1), 86–94.
- 880 Flynn, K. J., Davidson, K., Cunningham, A., 1996. Prey selection and re-
881 jection by a microflagellate; Implications for the study and operation of
882 microbial food webs. *J. Exp. Mar. Biol. Ecol.* 196 (1-2), 357–372.
- 883 Follows, M. J., Dutkiewicz, S., Grant, S., Chisholm, S. W., 2007. Emer-

884 gent biogeography of microbial communities in a model ocean. *Science*
885 315 (5820), 1843–1846.

886 Franks, P. J. S., 2002. NPZ models of plankton dynamics: Their construction,
887 coupling to physics, and application. *J. Oceanogr.* 58 (2), 379–387.

888 Furnas, M. J., 1990. In situ growth-rates of marine-phytoplankton - Ap-
889 proaches to measurement, community and species growth-rates. *J. Plank-*
890 *ton Research* 12 (6), 1117–1151.

891 Furnas, M. J., 1991. Net in situ growth rates of phytoplankton in an olig-
892 otrophic, tropical shelf ecosystem. *Limnol. Oceanogr.* 36 (1), 13–29.

893 Gallegos, C. L., Vant, W. N., 1996. An incubation procedure for estimating
894 carbon-to-chlorophyll ratios and growth-irradiance relationships of estuar-
895 ine phytoplankton. *Mar. Ecol. Prog. Ser.* 138 (1-3), 275–291.

896 Garrison, D. L., 1979. Monterey Bay phytoplankton I. Seasonal cycles of
897 phytoplankton assemblages. *J. Plankton Research* 1 (3), 241–266.

898 Geider, R. J., 1987. Light and temperature-dependence of the carbon to
899 chlorophyll-a ratio in microalgae and cyanobacteria - Implications for phys-
900 iology and growth of phytoplankton. *New Phytol.* 106 (1), 1–34.

901 Geider, R. J., La Roche, J., 2002. Redfield revisited: variability of C : N :
902 P in marine microalgae and its biochemical basis. *Eur. J. Phycol.* 37 (1),
903 1–17.

904 Gentleman, W., Leising, A., Frost, B., Strom, S., Murray, J., 2003. Func-

905 tional responses for zooplankton feeding on multiple resources: A review
 906 of assumptions and biological dynamics. *Deep-Sea Res. II* 50, 2847–2875.

907 Gruber, N., Frenzel, H., Doney, S. C., Marchesiello, P., McWilliams, J. C.,
 908 Moisan, J. R., Oram, J. J., Plattner, G. K., Stolzenbach, K. D., 2006.
 909 Eddy-resolving simulation of plankton ecosystem dynamics in the California
 910 Current System. *Deep-Sea Res. I* 53, 1483–1516.

911 Haidvogel, D. B., Beckman, A., 1999. *Numerical Ocean Circulation Model-*
 912 *ing*. Imperial Coll. Press, River Edge, N.J.

913 Harrison, W. G., 1976. Nitrate metabolism of red tide dinoflagellate
 914 *Gonyaulax-Polyedra* Stein. *J. Exp. Mar. Biol. Ecol.* 21 (3), 199–209.

915 Hickey, B. M., Banas, N. S., 2008. Why is the northern end of the California
 916 Current System so productive? *Oceanography* 21 (4), 90–107.

917 Hood, R. R., Abbott, M. R., Huyer, A., 1991. Phytoplankton and photosyn-
 918 thetic light response in the Coastal Transition Zone off Northern California
 919 in June 1987. *J. Geophys. Res.* 96, 14769–14780.

920 Hutchins, D. A., Bruland, K. W., 1998. Iron-limited diatom growth and Si :
 921 N uptake ratios in a coastal upwelling regime. *Nature* 393 (6685), 561–564.

922 Hutchinson, G. E., 1961. The paradox of the plankton. *Am. Nat.* 95 (882),
 923 137–145.

924 Johnson, Z. I., Zinser, E. R., Coe, A., McNulty, N. P., Woodward, E. M. S.,
 925 Chisholm, S. W., 2006. Niche partitioning among *Prochlorococcus* ecotypes
 926 along ocean-scale environmental gradients. *Science* 311 (5768), 1737–1740.

- 927 Leising, A. W., Pierson, J. J., Halsband-Lenk, C., Horner, R., Postel, J.,
928 2005a. Copepod grazing during spring blooms: Can *Pseudocalanus new-*
929 *mani* induce trophic cascades? *Prog. Oceanogr.* 67 (3-4), 406–421.
- 930 Leising, A. W., Pierson, J. J., Halsband-Lenk, C., Horner, R., Postel, J.,
931 2005b. Copepod grazing during spring blooms: Does *Calanus pacificus*
932 avoid harmful diatoms? *Prog. Oceanogr.* 67 (3-4), 384–405.
- 933 L’Helguen, S., Maguer, J.-F., Caradec, J., 2008. Inhibition kinetics of nitrate
934 uptake by ammonium in size-fractionated oceanic phytoplankton commu-
935 nities: implications for new production and f-ratio estimates. *J. Plankton*
936 *Research* 30 (10), 1179–1188.
- 937 Litchman, E., Klausmeier, C. A., Miller, J. R., Schofield, O. M., Falkowski,
938 P. G., 2006. Multi-nutrient, multi-group model of present and future
939 oceanic phytoplankton communities. *Biogeosciences* 3 (4), 585–606.
- 940 Litchman, E., Klausmeier, C. A., Schofield, O. M., Falkowski, P. G., 2007.
941 The role of functional traits and trade-offs in structuring phytoplankton
942 communities: Scaling from cellular to ecosystem level. *Ecol. Lett.* 10, 1170–
943 1181.
- 944 Marra, J., Barber, R. T., 2004. Phytoplankton and heterotrophic respiration
945 in the surface layer of the ocean. *Geophys. Res. Lett.* 31 (9).
- 946 Moore, J. K., Doney, S. C., Kleypas, J. A., Glover, D. M., Fung, I. Y.,
947 2002a. An intermediate complexity marine ecosystem model for the global
948 domain. *Deep-Sea Res. II* 49 (1-3), 403–462.

- 949 Moore, L. R., Post, A. F., Rocap, G., Chisholm, S. W., 2002b. Utilization
950 of different nitrogen sources by the marine cyanobacteria *Prochlorococcus*
951 and *Synechococcus*. *Limnol. Oceanogr.* 47 (4), 989–996.
- 952 Nianzhi, J., 1993. Interactions between ammonium uptake and nitrate uptake
953 by natural phytoplankton assemblages. *Chin. J. Oceanol. Limnol.* 11 (2),
954 97–107.
- 955 O'Reilly, J. E., Maritorena, S., Mitchell, B. G., Siegel, D. A., Carder, K. L.,
956 Garver, S. A., Kahru, M., McClain, C., 1998. Ocean color chlorophyll
957 algorithms for SeaWiFS. *J. Geophys. Res.* 103 (C11), 24937–24953.
- 958 Plattner, G. K., Gruber, N., Frenzel, H., McWilliams, J. C., 2005. Decou-
959 pling marine export production from new production. *Geophys. Res. Lett.*
960 32 (11).
- 961 Putland, J. N., Iverson, R. L., 2007. Phytoplankton biomass in a subtropical
962 estuary: Distribution, size composition, and carbon : chlorophyll ratios.
963 *Estuaries and Coasts* 30 (5), 878–885.
- 964 Rabouille, S., Edwards, C. A., Zehr, J. P., 2007. Modelling the vertical dis-
965 tribution of *Prochlorococcus* and *Synechococcus* in the North Pacic Sub-
966 tropical Ocean. *Environ. Microbiol.* 9, 2588–2602.
- 967 Riemann, B., Simonsen, P., Stensgaard, L., 1989. The carbon and chloro-
968 phyll content of phytoplankton from various nutrient regimes. *J. Plankton*
969 *Research* 11 (5), 1037–1045.
- 970 Roy, S., Chattopadhyay, J., 2007. Enrichment and ecosystem stability: Effect
971 of toxic food. *Biosystems* 90 (1), 151–160.

972 Sathyendranath, S., Stuart, V., Nair, A., Oka, K., Nakane, T., Bouman, H.,
973 Forget, M.-H., Maass, H., Platt, T., 2009. Carbon-to-chlorophyll ratio and
974 growth rate of phytoplankton in the sea. *Mar. Ecol. Prog. Ser.* 383, 73–84.

975 Sherr, E. B., Sherr, B. F., Wheeler, P. A., 2005. Distribution of coccoid
976 cyanobacteria and small eukaryotic phytoplankton in the upwelling ecosys-
977 tem off the Oregon coast during 2001 and 2002. *Deep-Sea Res. II* 52 (1-2),
978 317–330.

979 Smolarkiewicz, P. K., Margolin, L. G., 1998. MPDATA: A finite-difference
980 solver for geophysical flows. *J. Comput. Phys.* 140 (2), 459–480.

981 Spitz, Y. H., Newberger, P. A., Allen, J. S., 2003. Ecosystem response to
982 upwelling off the Oregon coast: Behavior of three nitrogen-based models.
983 *J. Geophys. Res. C* 108.

984 Strub, P. T., Allen, J. S., Huyer, A., Smith, R. L., 1987. Large-scale structure
985 of the spring transition in the coastal ocean off western North America. *J.*
986 *Geophys. Res.* 92, 1527–1544.

987 Taylor, K. E., 2001. Summarizing multiple aspects of model performance in
988 a single diagram. *J. Geophys. Res. D* 106 (D7), 7183–7192.

989 Veldhuis, M. J. W., Kraay, G. W., 2004. Phytoplankton in the subtropical
990 Atlantic ocean: towards a better assessment of biomass and composition.
991 *Deep-Sea Res. I* 51 (4), 507–530.

992 Veldhuis, M. J. W., Timmermans, K. R., Croot, P., van der Wagt, B., 2005.
993 Picophytoplankton; a comparative study of their biochemical composition
994 and photosynthetic properties. *J. Sea Res.* 53 (1-2), 7–24.

- 995 Veneziani, M., Edwards, C. A., Doyle, J. D., Foley, D., 2009a. A central Cal-
996 ifornia coastal ocean modeling study: 1. Forward model and the influence
997 of realistic versus climatological forcing. J. Geophys. Res. C 114.
- 998 Veneziani, M., Edwards, C. A., Moore, A. M., 2009b. A central California
999 coastal ocean modeling study: 2. Adjoint sensitivities to local and remote
1000 forcing mechanisms. J. Geophys. Res. C 114.
- 1001 Venrick, E. L., 2009. Floral patterns in the California Current: The coastal-
1002 offshore boundary zone. J. Mar. Res. 67 (1), 89–111.
- 1003 Verity, P. G., Smetacek, V., 1996. Organism life cycles, predation, and the
1004 structure of marine pelagic ecosystems. Mar. Ecol. Prog. Ser. 130 (1-3),
1005 277–293.
- 1006 Weiler, C. S., Eppley, R. W., 1979. Temporal pattern of division in the
1007 dinoflagellate genus *Ceratium* and its application to the determination of
1008 growth rate. J. Exp. Mar. Biol. Ecol. 39 (1), 1–24.
- 1009 Worden, A. Z., Nolan, J. K., Palenik, B., 2004. Assessing the dynamics and
1010 ecology of marine picophytoplankton: The importance of the eukaryotic
1011 component. Limnol. Oceanogr. 49 (1), 168–179.

Table A.1: Phytoplankton parameters for Prochlorococcus-like (PLP), small non-Prochlorococcus-like (SNP), large non-diatoms (LND), and diatom functional groups.

Parameter Description	Symbol	unit	PLP	SNP	LND	diatom
Values Governing Randomized Parameters						
Phosphate half saturation constant (min,max)	k_{PO_4}	$\mu\text{M P}$	0.010, 0.005	0.015, 0.02	0.035, 0.02	0.035, 0.02
Nitrate half saturation constant (min,max)	k_{NO_3}	$\mu\text{M N}$	0.16, 0.08	0.24, 0.32	0.56, 0.32	0.56, 0.32
Nitrite half saturation constant (min,max)	k_{NO_2}	$\mu\text{M N}$	0.16, 0.08	0.24, 0.32	0.56, 0.32	0.56, 0.32
Ammonium half saturation constant (min,max)	k_{NH_4}	$\mu\text{M N}$	0.08, 0.04	0.12, 0.16	0.28, 0.16	0.28, 0.16
Silicic acid half saturation constant	k_{Si}	$\mu\text{M Si}$	-	-	-	1
PAR half-saturation (mean, standard deviation)	k_{par}	$(\text{W m}^{-2})^{-1}$	0.012, 0.02	0.012, 0.02	0.012, 0.006	0.012, 0.006
PAR inhibition (mean, standard deviation)	k_{inh}	$(\text{W m}^{-2})^{-1}$	0.006, 1e-4	0.006, 1e-4	0.001, 5e-5	0.001, 5e-5
Temperature optimum coefficient (min,max)	T_o	$^{\circ}\text{C}$	5, 25	5, 25	5, 25	5, 25
Other Fixed Parameters						
Maximum growth rate	μ	d^{-1}	2.8	2.8	4.0	5.0
Temperature coefficient a	c_a	-	0.333	0.333	0.333	0.333
Temperature coefficient b	c_b	-	0.001	0.001	0.0003	0.0003
Temperature decay exponent	τ	-	4.000	4.000	4.000	4.000
Temperature decay scale	T_d	$^{\circ}\text{C}$	1.010	1.010	1.010	1.010
Temperature normalization coefficient	T_n	-	0.300	0.300	0.300	0.300
Ammonium inhibition coefficient	σ_A	$(\mu\text{M N})^{-1}$	4.6	4.6	4.6	4.6
Si:P elemental ratio	r_{SiP}	mol Si:mol P	-	-	-	16
N:P elemental ratio	r_{NP}	mol N:mol P	16	16	16	16
C:Chl	r_{CChl}	g C:g chl	300	300	100	50
Phytoplankton sinking rate	$w^{(P)}$	m d^{-1}	0.0	0.0	0.5	0.5
Phytoplankton mortality rate	$m^{(P)}$	d^{-1}	0.1	0.1	0.1	0.1
Fraction of P mortality exported to particulates	$E^{(P)}$	-	0.2	0.2	0.5	0.5
Palatability by microzooplankton	$\pi^{(P)}$	-	1	1	0.4	0.4
Palatability by mesozooplankton	$\pi^{(P)}$	-	0.2	0.2	1	0.7
Grazing assimilation efficiency by microzoo	$\alpha^{(P)}$	-	0.500	0.500	0.200	0.200
Grazing assimilation efficiency by mesozoo	$\alpha^{(P)}$	-	0.700	0.700	0.500	0.500

Table A.2: Zooplankton parameters for microzooplankton and mesozoo-plankton.

Parameter Description	Symbol	unit	Microzoo	Mesozoo
Half saturation constant for grazing	k_g	$\mu\text{M P}$	0.04	0.07
Maximum grazing rate	G^{max}	d^{-1}	1.0	0.5
Grazing assimilation efficiency by mesozoo	$\alpha^{(Z)}$	-	0.3	-
Fraction of unassimilated prey exported to particulates	$E^{(G)}$	-	0.8	0.8
Zooplankton mortality	$m^{(Z)}$	d^{-1}	0.033	0.033
Fraction of Z mortality exported to particulates	$E^{(Z)}$	-	0.2	0.7

Table A.3: Other parameterizations: remineralization of dissolved and particulate organic matter, nitrification, and light attenuation.

Parameter Description	Symbol	unit	Value
DOP remineralization rate	k_{dop}	d^{-1}	0.020
DON remineralization rate	k_{don}	d^{-1}	0.020
POP remineralization rate	k_{dop}	d^{-1}	0.033
PON remineralization rate	k_{don}	d^{-1}	0.033
PSi remineralization rate	k_{Psi}	d^{-1}	0.003
POM sinking rate	w_{pom}	m d^{-1}	10
NH4 to NO2 oxidation rate	k_A	d^{-1}	0.1
NO2 to NO3 oxidation rate	k_B	d^{-1}	0.033
Critical light level below which oxidation occurs	I_0	W m^{-2}	10
PAR attenuation coefficient	k_o	m^{-1}	0.04
PAR attenuation coefficient from phytoplankton	k_p	$(\mu\text{M P m})^{-1}$	0.06

1012 **List of Figures**

1013	1	Ecosystem model conceptual diagram. Boxes represent differ-	
1014		ent state variables. Colors correspond to nutrient type. Ar-	
1015		rows represent processes as labeled. The subscript n refers	
1016		to the specific nutrient for DOM, POM, Zoo and Phyto state	
1017		variables. The subscript i and j represent the index of phyto-	
1018		plankton or zooplankton analog.	56
1019	2	Left axis: Time series of phytoplankton biomass for a model of	
1020		phytoplankton subject to growth and respiration under con-	
1021		tinuous irradiance (dashed) and with a 12-hour on/12-hour	
1022		off cycle (solid). Growth rate is 1.4 d^{-1} (2.8 d^{-1}) for dashed	
1023		(solid) growth curve. Right axis: light limitation factor that	
1024		corresponds to solid curve.	57
1025	3	Log_{10} of the five-year average (2000-2005) chlorophyll concen-	
1026		tration (mg m^{-3}) from (a) model surface level and (b) SeaW-	
1027		iFS chlorophyll estimate. Model line along (but longer than)	
1028		CalCOFI Line 67 is displayed in (a).	58

1029	4	Taylor diagrams for (a) 5-year average (2000-2004) and (b)	
1030		seasonal mean chlorophyll concentrations (mg m^{-3}) of model	
1031		surface level and SeaWiFS observations. In (a) calculations	
1032		for the entire domain (DOMAIN), coastal and offshore re-	
1033		gions (Cst and Off), and Northern and Southern coastal (N	
1034		Cst and S Cst) and offshore (N Cst and S Cst) regions. North	
1035		and South regions are divided by latitude 40.5°N , and coastal	
1036		and offshore regions are on either side of the 1000 m isobath.	
1037		Bias for each comparison is given in parentheses. In (b), all	
1038		calculations are for entire domain.	59
1039	5	Five-year average from model surface for (a) diatoms, (b)	
1040		LND, (c) SNP, (d) PLP, (e) microzooplankton, (f) mesozoo-	
1041		plankton. (a-d) show chlorophyll in mg chl m^{-3} , and (e-f)	
1042		present biomass in terms of $\mu\text{mole P l}^{-1}$	60
1043	6	Five-year average chlorophyll concentration (mg m^{-3}) from	
1044		model surface for each of the top 3 dominant subgroups for	
1045		PLP (a, b, c) and the top 2 dominant subgroups for SNP (d, e).	61
1046	7	Log_{10} of the monthly averages of modeled total chlorophyll	
1047		concentration (mg chl m^{-3}) at surface.	62

1048	8	Monthly averages of modeled total chlorophyll concentration	
1049		(mg chl m ⁻³) along line in Figure 3 in the upper 200 m.	
1050		Monthly minimum and maximum are shown in brackets. Note	
1051		that maximum values in a few months exceed the grayscale.	
1052		The dashed contour occurs at 0.05 mg m ⁻³ . The contour in-	
1053		terval for the solid contours is 0.2 mg m ⁻³ , beginning at a	
1054		value of 0.1 m ⁻³	63
1055	9	Monthly averages of modeled chlorophyll concentration along	
1056		line shown in Figure 3 for the most abundant (a, b) and second	
1057		most abundant (c, d) PLP subtypes during the months of July	
1058		(left column) and August (right column). Dashed contour	
1059		occurs at 0.001 mg chl m ⁻³ . Heavy solid contour levels begin	
1060		at and occur every 0.005 mg chl m ⁻³ . Light solid line at right	
1061		indicates topography.	64
1062	10	Time-series of average modeled biomass in near surface waters	
1063		for (a) total phytoplankton (blue) and small phytoplankton	
1064		(green), (b) diatoms (blue) and LND (green), (c) PLP (blue)	
1065		and SNP (green), and (d) microzooplankton (blue) and meso-	
1066		zooplankton (green). All modeled fields are in units of μ M	
1067		P.	65
1068	11	Time-series of average modeled biomass in near surface waters	
1069		for the most abundant (a) diatoms, (b) LND, (c) SNP, and (d)	
1070		PLP subtypes. Biomass units are mg chl m ⁻³	66

1071	12	Taylor diagram for the year 2000 annual mean chlorophyll con-	
1072		centration (mg m^{-3}) in near surface waters of model output	
1073		and SeaWiFS observations across five randomized runs. Run	
1074		1 is that used throughout the manuscript. The bias for each	
1075		comparison is given in parentheses.	67

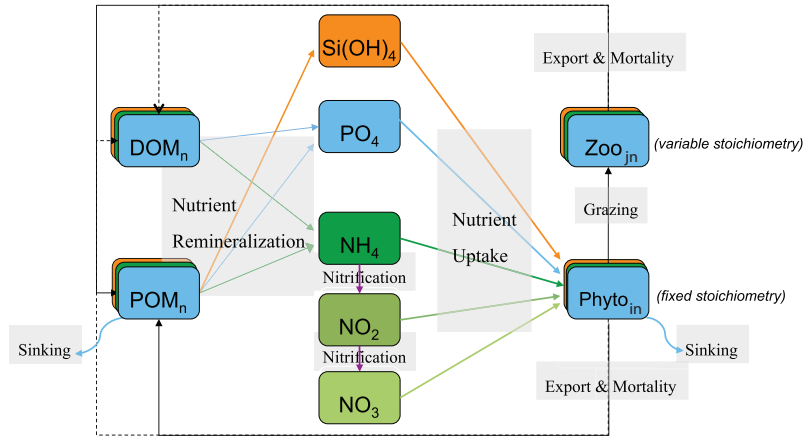


Figure 1: Ecosystem model conceptual diagram. Boxes represent different state variables. Colors correspond to nutrient type. Arrows represent processes as labeled. The subscript n refers to the specific nutrient for DOM, POM, Zoo and Phyto state variables. The subscript i and j represent the index of phytoplankton or zooplankton analog.

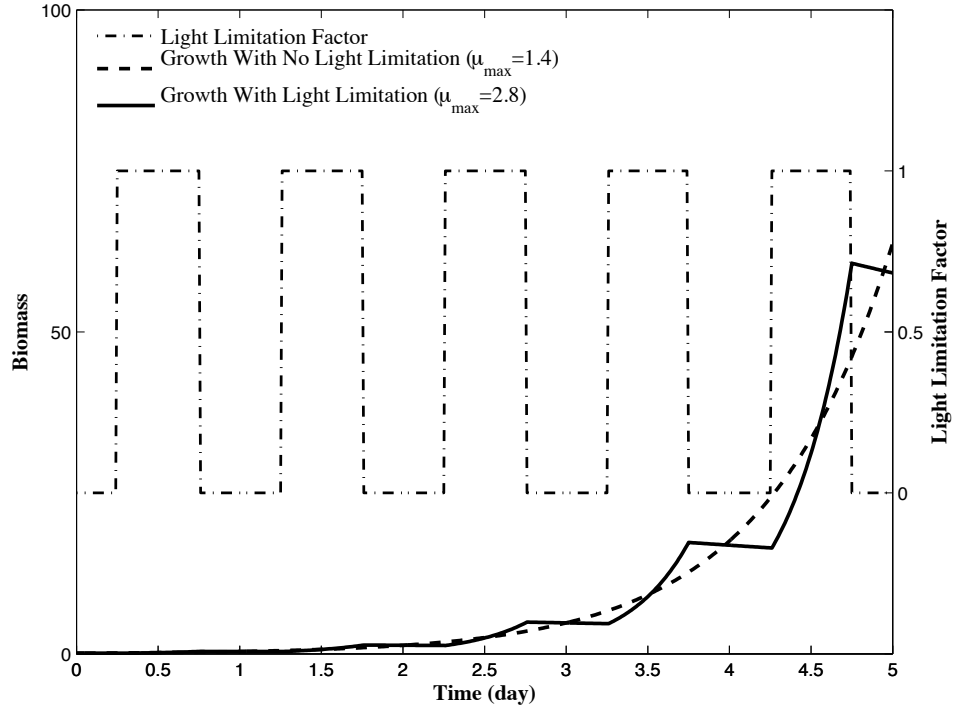


Figure 2: Left axis: Time series of phytoplankton biomass for a model of phytoplankton subject to growth and respiration under continuous irradiance (dashed) and with a 12-hour on/12-hour off cycle (solid). Growth rate is 1.4 d^{-1} (2.8 d^{-1}) for dashed (solid) growth curve. Right axis: light limitation factor that corresponds to solid curve.

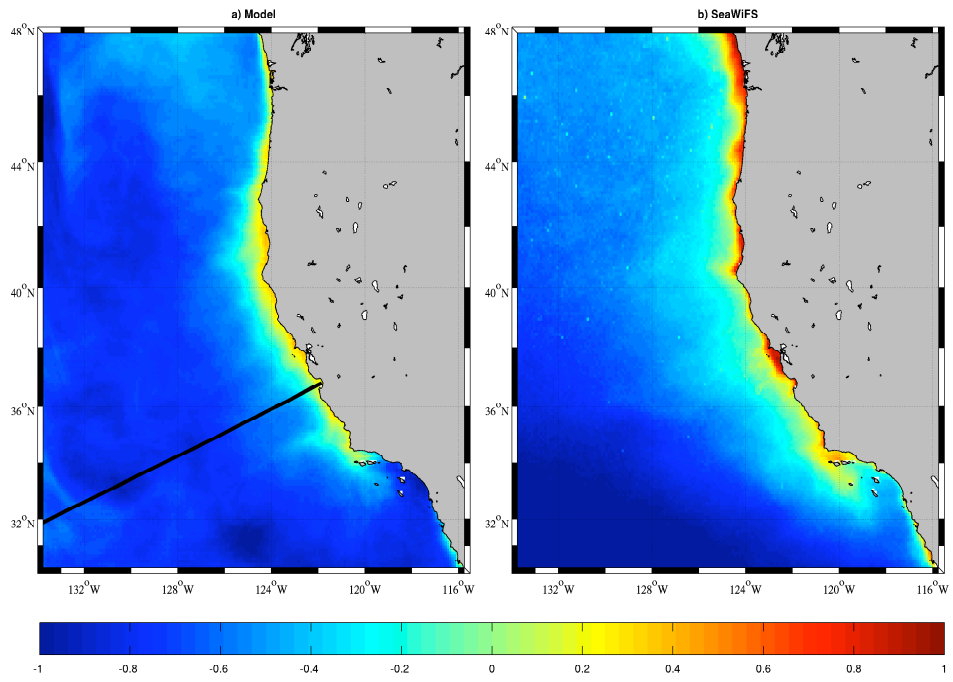


Figure 3: Log_{10} of the five-year average (2000-2005) chlorophyll concentration (mg m^{-3}) from (a) model surface level and (b) SeaWiFS chlorophyll estimate. Model line along (but longer than) CalCOFI Line 67 is displayed in (a).

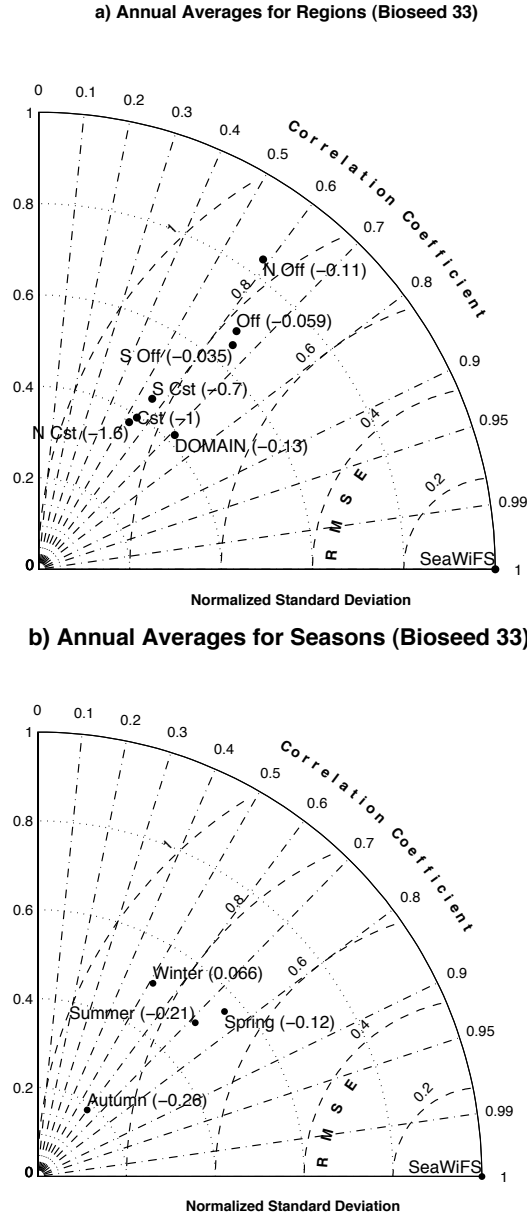


Figure 4: Taylor diagrams for (a) 5-year average (2000-2004) and (b) seasonal mean chlorophyll concentrations (mg m^{-3}) of model surface level and SeaWiFS observations. In (a) calculations for the entire domain (DOMAIN), coastal and offshore regions (Cst and Off), and Northern and Southern coastal (N Cst and S Cst) and offshore (N Cst and S Cst) regions. North and South regions are divided by latitude 40.5°N , and coastal and offshore regions are on either side of the 1000 m isobath. Bias for each comparison is given in parentheses. In (b), all calculations are for entire domain.

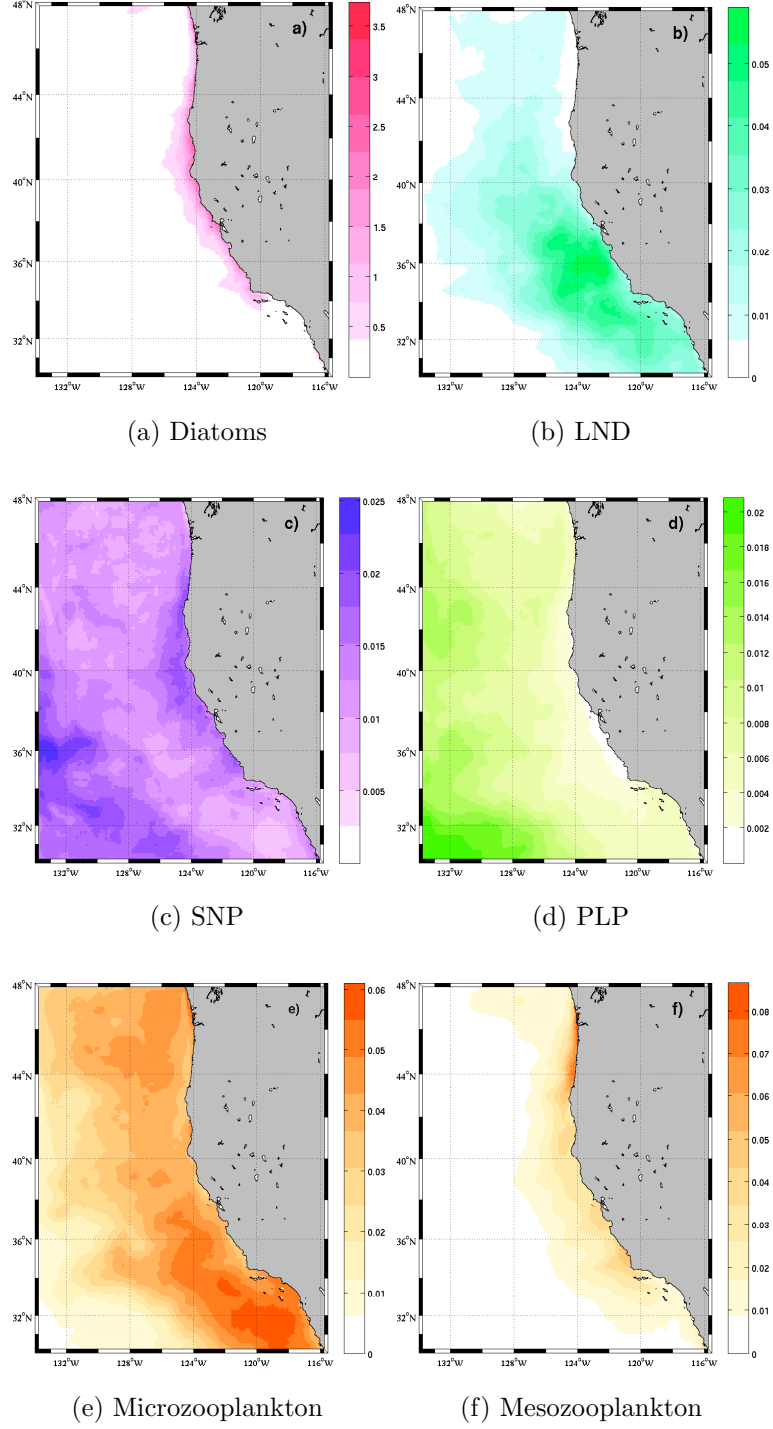


Figure 5: Five-year average from model surface for (a) diatoms, (b) LND, (c) SNP, (d) PLP, (e) microzooplankton, (f) mesozooplankton. (a-d) show chlorophyll in mg chl m^{-3} , and (e-f) present biomass in terms of $\mu\text{mole P l}^{-1}$.

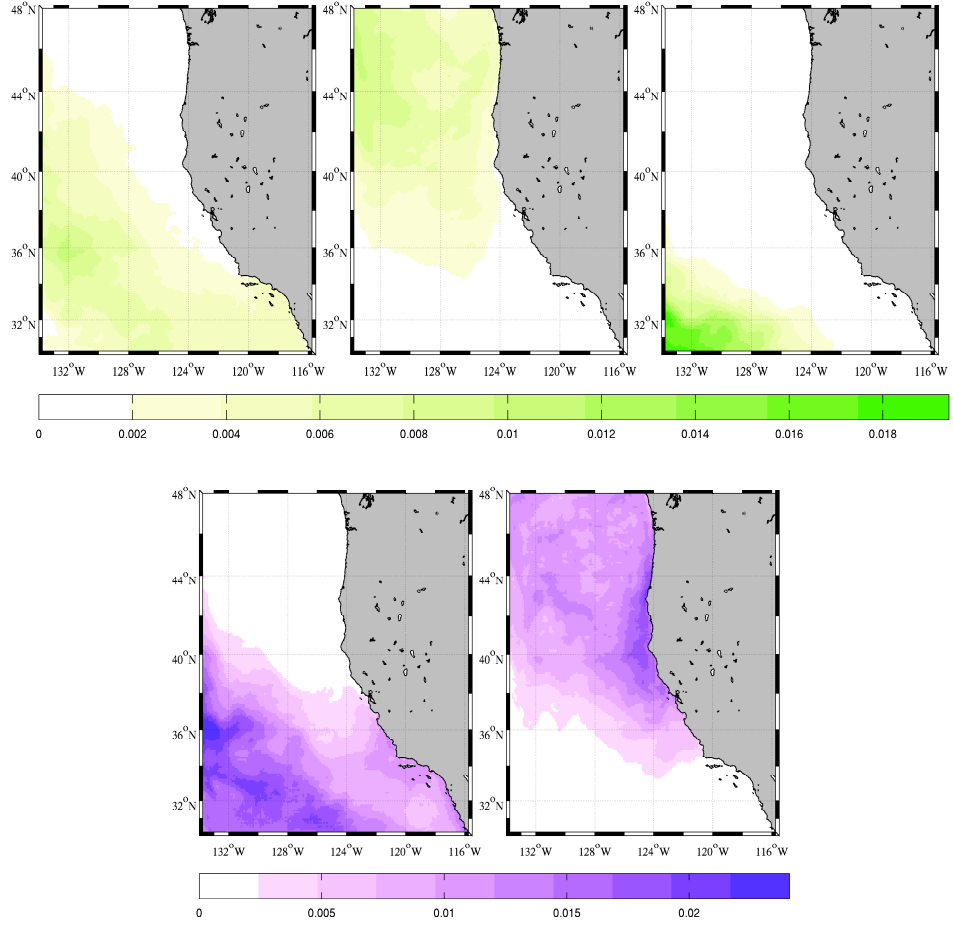


Figure 6: Five-year average chlorophyll concentration (mg m^{-3}) from model surface for each of the top 3 dominant subgroups for PLP (upper panel: a, b, c) and the top 2 dominant subgroups for SNP (lower panel: d, e).

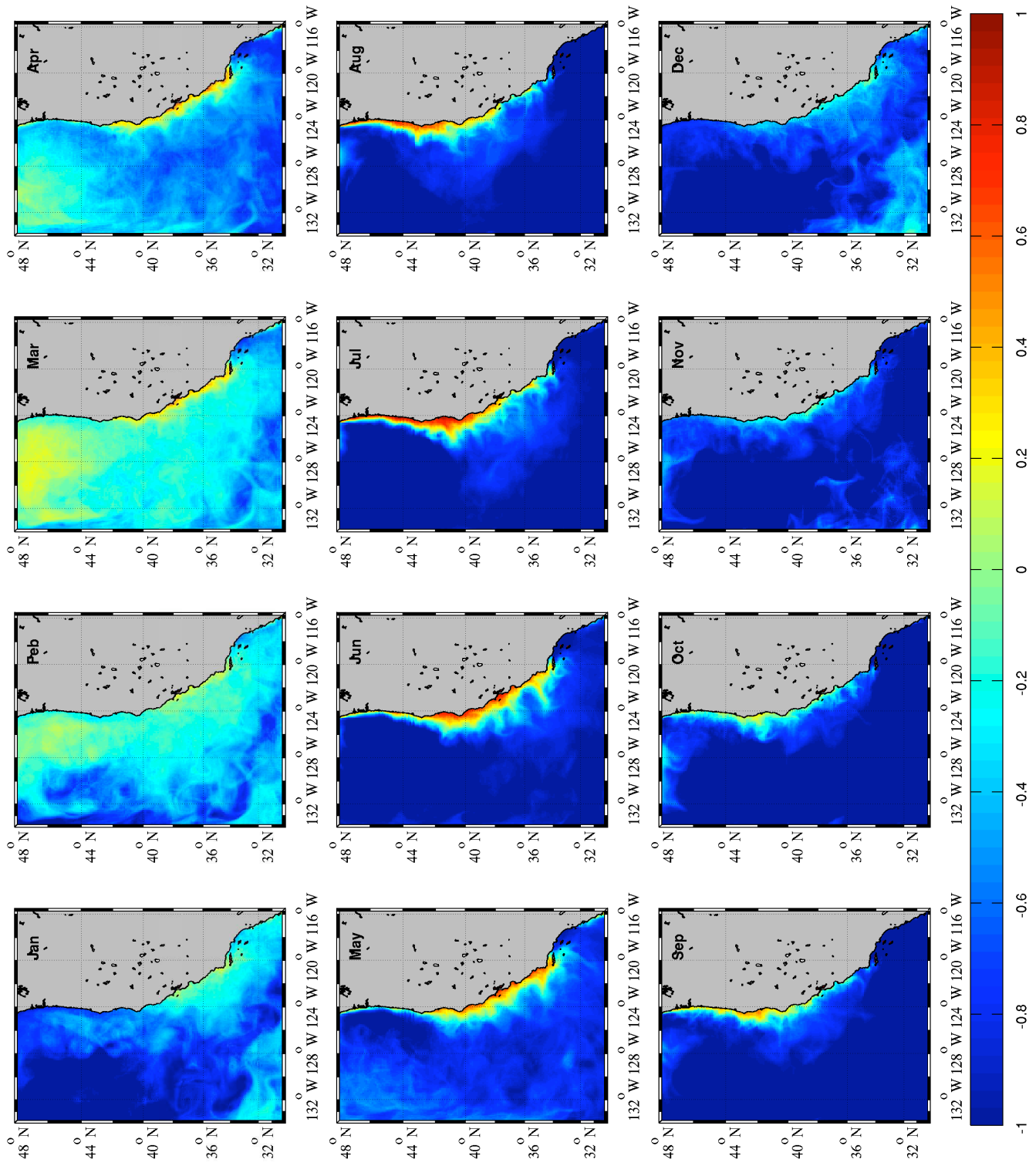


Figure 7: Log₁₀ of the monthly averages of modeled total chlorophyll concentration (mg chl m⁻³) at surface.

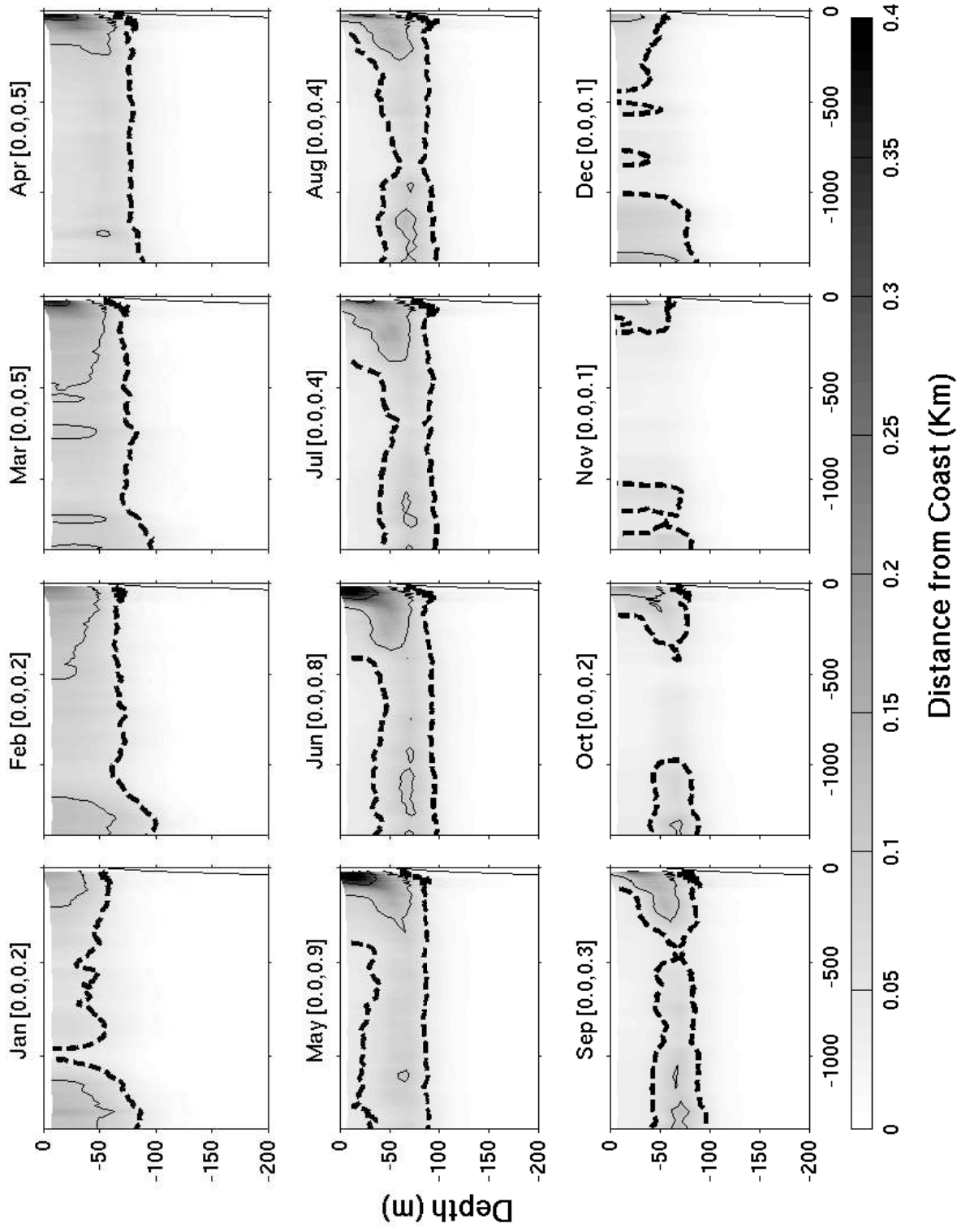


Figure 8: Monthly averages of modeled total chlorophyll concentration (mg chl m⁻³) along line in Figure 3 in the upper 200 m. Monthly minimum and maximum are shown in brackets. Note that maximum values in a few months exceed the grayscale. The dashed contour occurs at 0.05 mg m⁻³. The contour interval for the solid contours is 0.2 mg m⁻³, beginning at a value of 0.1 m⁻³.

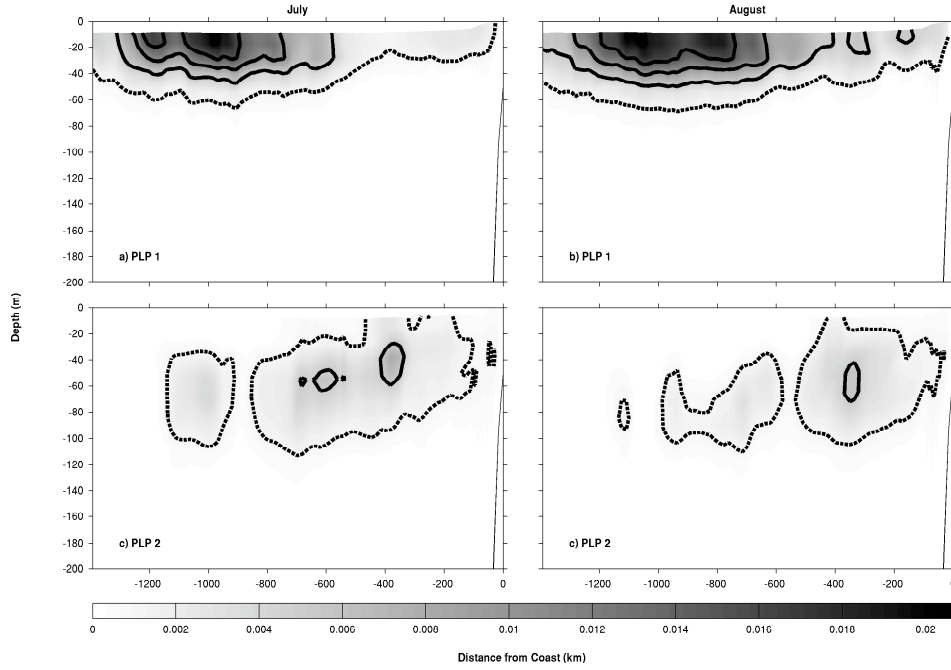


Figure 9: Monthly averages of modeled chlorophyll concentration along line shown in Figure 3 for the most abundant (a, b) and second most abundant (c, d) PLP subtypes during the months of July (left column) and August (right column). Dashed contour occurs at $0.001 \text{ mg chl m}^{-3}$. Heavy solid contour levels begin at and occur every $0.005 \text{ mg chl m}^{-3}$. Light solid line at right indicates topography.

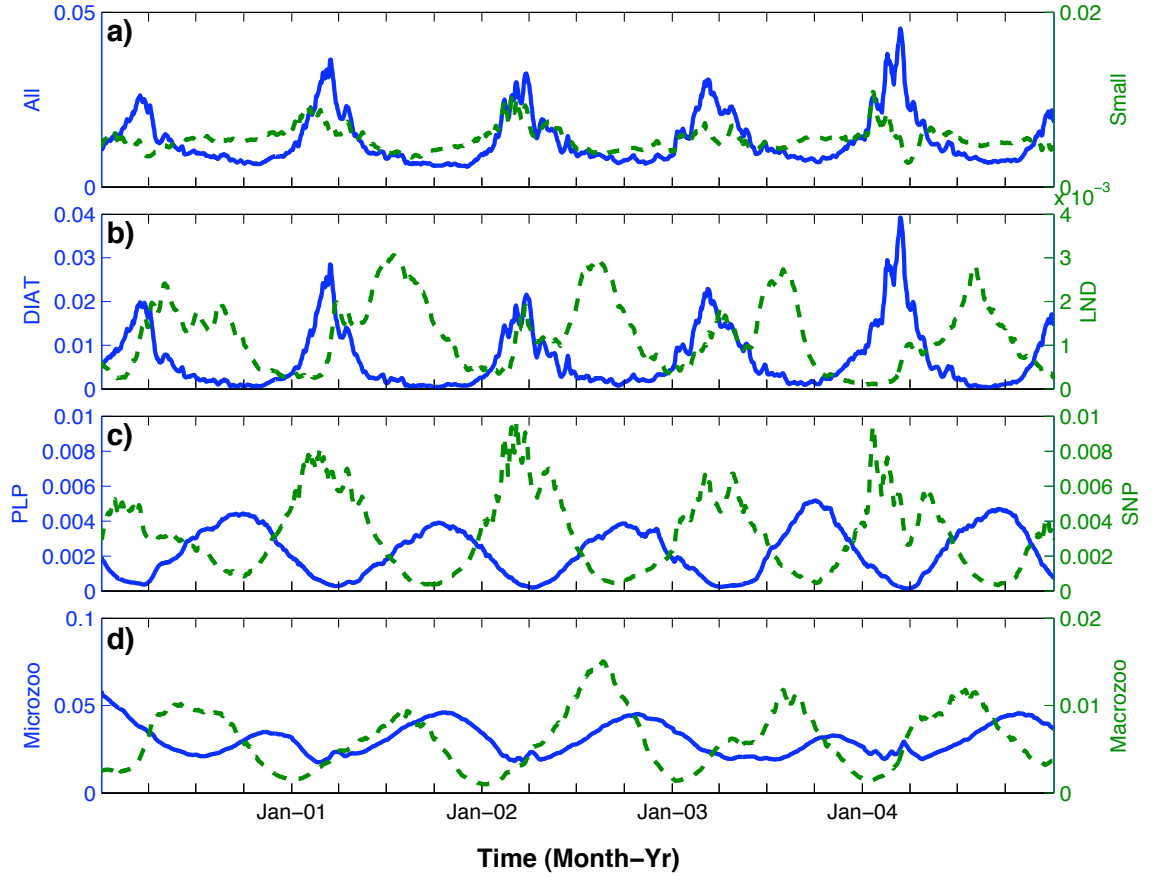


Figure 10: Time-series of average modeled biomass in near surface waters for (a) total phytoplankton (blue) and small phytoplankton (green), (b) diatoms (blue) and LND (green), (c) PLP (blue) and SNP (green), and (d) microzooplankton (blue) and mesozooplankton (green). All modeled fields are in units of $\mu\text{M P}$.

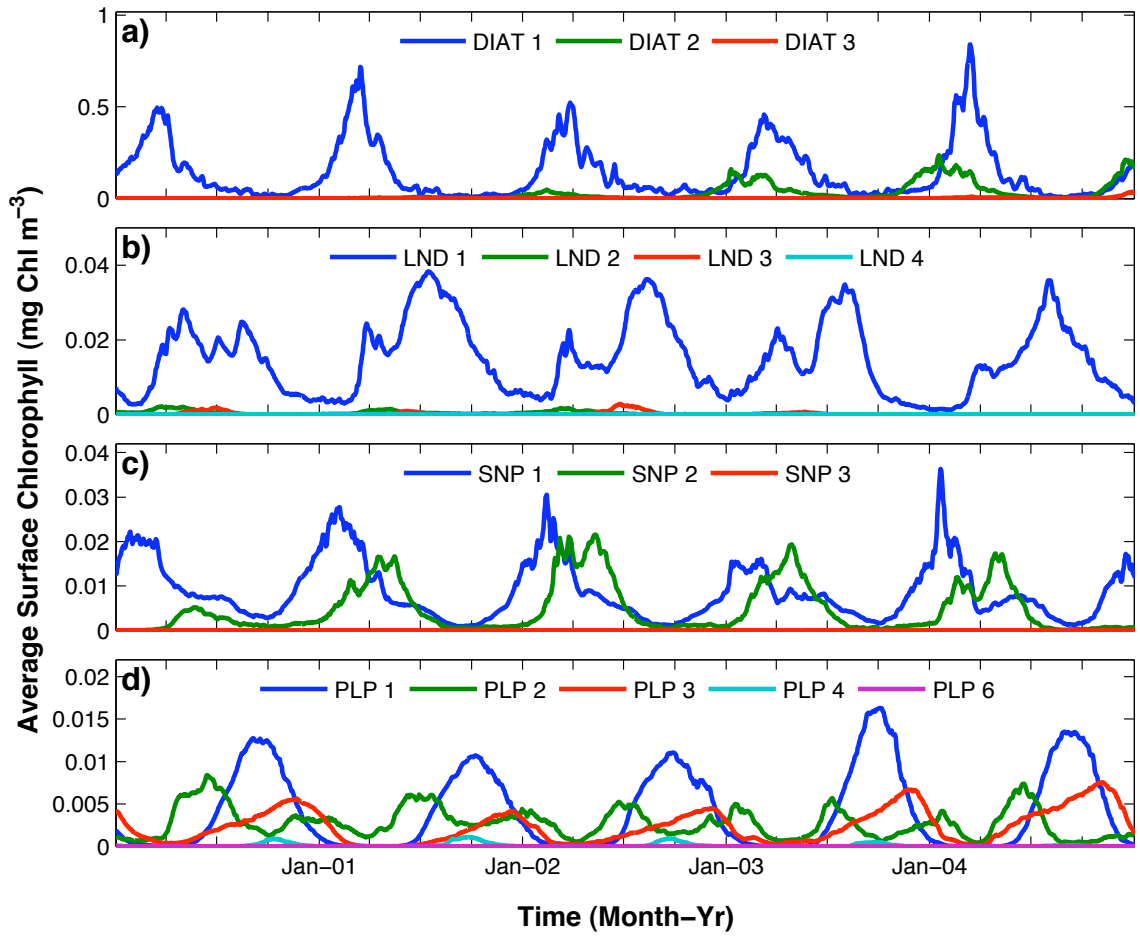


Figure 11: Time-series of average modeled biomass in near surface waters for the most abundant (a) diatoms, (b) LND, (c) SNP, and (d) PLP subtypes. Biomass units are mg chl m⁻³.

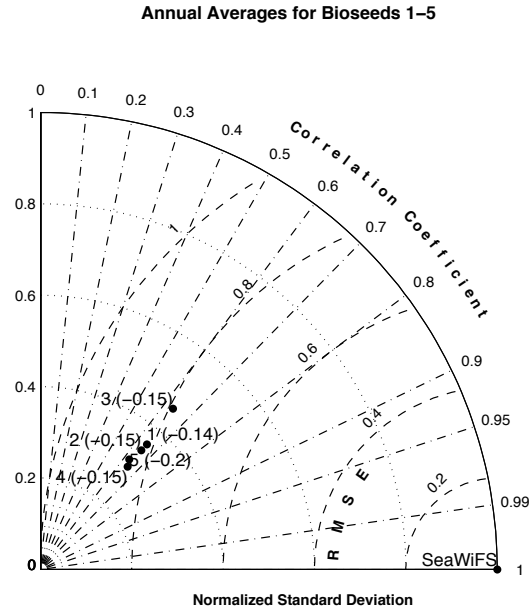


Figure 12: Taylor diagram for the year 2000 annual mean chlorophyll concentration (mg m^{-3}) in near surface waters of model output and SeaWiFS observations across five randomized runs. Run 1 is that used throughout the manuscript. The bias for each comparison is given in parentheses.